FERMILAB-PUB-08-337-E

The Development of Superconducting Magnets for Use in Particle Accelerators: From the Tevatron to the LHC

Alvin Tollestrup

Fermil National Accelerator Laboratory,
P. O. Box 500, Batavia, Illinois 60510, USA
alvin@fnal.gov

Ezio Todesco

CERN, Accelerator Technology Department,
Geneva, 1211 Switzerland
ezio.todesco@cern.ch

Superconducting magnets have played a key role in advancing the energy reach of proton synchrotrons and enabling them to play a major role in defining the Standard Model. The problems encountered and solved at the Tevatron are described and used as an introduction to the many challenges posed by the use of this technology. The LHC is being prepared to answer the many questions beyond the Standard Model and in itself is at the cutting edge of technology. A description of its magnets and their properties is given to illustrate the advances that have been made in the use of superconducting magnets over the last 30 years.

1. Introduction

Superconductivity has played a key role in the development of magnets for the accelerators used in high energy physics. And yet, as we shall see, it is at best an unholy alliance! The challenge for the last 60 years has always been to push accelerators to higher energy and in general this has paid off with exciting and often unexpected results.

Table 1 lists the accelerators that we will consider in this article along with the beam energy, magnetic field strength and machine circumference. The Tevatron was the first successful synchrotron using superconducting magnets and will be used to illustrate the many difficult problems that had to be overcome. A detailed description of the Large Hadron Collider (LHC) will be used to show the state-of-the-art technology. There is an inevitable change in style brought about by this approach and the authors hope that the reader will either enjoy the approach or forgive the authors.

Table 1. Four accelerators using superconducting magnets and their major parameters.

	E (GeV)	B (T)	Length (m)	First beam
Tevatron	980	4.3	6280	7 1983
HERA	920	5.0	6336	4 1991
RHIC	100/n	3.5	3834	6 2000
LHC	7000	8.3	26659	8 2008

To understand why superconductivity has played such a pivotal role in accelerator development, consider the landscape in the 1970s. The Standard Model was beginning to emerge but important pieces were missing. The Fermilab Main Ring was the largest operating proton synchrotron with a radius of 1 km, a peak field of 2 T, a power consumption of more than 50 MW and an operating energy of 400 GeV. Type II superconductors were becoming available that offered the prospect of operating at fields of more than 4 T with no resistive losses. The possibility of doubling the energy of the Fermilab accelerator and at the same time reducing the power consumption was irresistible to Robert R. Wilson, the founding director of the laboratory. The original contract for the laboratory did not specifically define the machine that was to be built, only the total cost. He was in the enviable position of having constructed the laboratory and its accelerator under budget by about US$30 million and his plan was to use the excess money to build a second superconducting ring with

1 TeV energy. A feeling for the environment in which the Tevatron was conceived can be gleaned from the following paragraph from Ref. 1.

"The design process, and if carried out, the construction of the Doubler, builds upon our experience at NAL. We have not proceeded on the basis of deciding what is readily practicable, designing to that, adding up the cost and attempting the result. Instead, we have set a cost goal and keep designing, redesigning, haggling and improving until we have done what we set out to do. Occasionally, we are forced to admit that we are not clever enough to achieve our cost goal and admit defeat, but not without a struggle." A nice contrast with the present process of building a new machine! (Note: In most of this article we will refer to the Tevatron even though in its early stages it was called the Doubler or the Energy Saver.)

During this period there was active investigation for using this new technology at many other high energy physics laboratories. A 4 GeV experimental ring, ESCAR [2], was under construction at LBL. Brookhaven was developing a 400 × 400 GeV pp collider called ISABELLE [3], and Rutherford Lab [4] did some crucial development of superconducting cable while studying the possibility of building the SPS with superconducting magnets, an effort that was discarded in favor of conventional (i.e. warm) magnet technology.

The Tevatron was first commissioned in 1983 as a fixed-target machine that accelerated protons to peak energy and extracted them to a target where they produced secondary beams of particles [5]. However, the spectacular success at CERN with its pbar-proton collider shifted the emphasis to using the large rings in the collider mode. This was first achieved at the Tevatron in 1986 and all of the other rings in Table 1 have been initially designed for use in this mode. The availability of superconducting cable has had a dramatic impact on accelerator design and that will now be explored.

2. Superconducting Accelerator Magnets

Normal magnets use iron to shape the field and water-cooled copper coils to supply the ampere turns. The current density in practical magnets is of the order of 5 A/mm^2 or less due to the difficulty of removing the joule heating. In contrast,

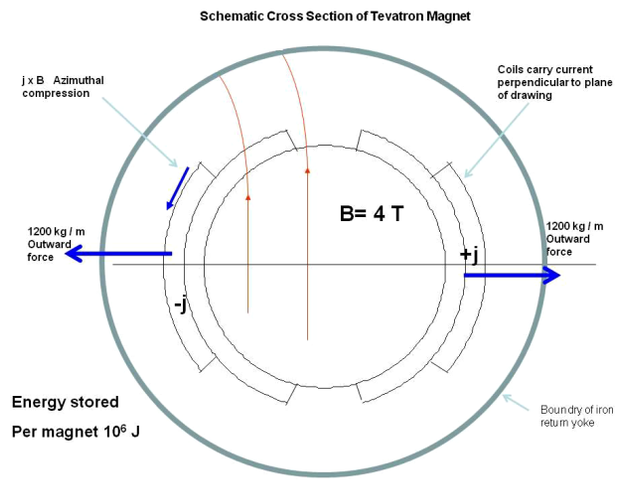

Fig. 1. Schematic drawing of the Tevatron dipole magnet transverse cross-section, showing the configuration of the coil and iron return yoke as well as the direction of some of the forces acting on the coil.

superconducting cable can operate at current densities more than 100 times greater. This offers the possibility of designing magnets whose field shape is governed by the geometry of the current-carrying conductors and the iron plays a secondary role of providing a flux return and shielding for the external space [6]. Figure 1 shows a very abstract schematic of the Tevatron dipole cross section.

The design is based on the superposition of two simple solutions to Maxwell's equations. If the field is expanded in cylindrical coordinates, it is easy to show that a current sheet with the current flowing in the longitudinal direction and in which the density varies as the cosine of the angle in the transverse plane (i.e. the so-called cosθ layout [4]) will produce a uniform dipole field inside. If this current sheet is inserted in a coaxial iron return yoke, the field induced in the iron produces a uniform field within the cylindrical hole and adds to the uniform field within the current sheet. The current density is picked to give the desired field inside the coil and the radius of the hole in the yoke is picked to give a peak field at the pole that is less than saturation. In the Tevatron, the iron provides about 18% of the central field.

A number of choices were made that were not necessary in later accelerators. The diameter of the beam tube is 76.2 mm and the diameter of the hole in the yoke is about 250 mm and the current density is such that the field in the center is about 4 T.

By keeping the field in the iron below saturation, the field is proportional to the current. In the Tevatron the quadrupoles and dipoles are all in series and so it is important to have the fields track each other during acceleration. In addition, the yoke is at room temperature and the coil must be held at liquid helium temperature, and so there is a cryostat that fits in the space between the coil and the yoke. The yoke is thus not available to support the large magnetically induced forces. We will discuss these choices later but now we must discuss some properties of superconductors.

2.1. *Superconductors*

The gross properties of a superconducting cable are contained in a graph of current density versus critical field. If the current density exceeds the critical value, the superconducting state is destroyed and one says that the conductor "goes normal" or "quenches." This is shown in Fig. 2 for Nb–Ti at 1.8 K and 4.6 K.

On this same plot one can show the load line of the magnet which is the relation in the magnet between current density in the winding and the high field point at the conductor. The case shown is for a magnet with an operating high field point of 4 T and operated at 4.6 K. If the current is raised past the quench point, or if the ambient temperature should increase, the magnet would quench. The term "short sample limit" is used to characterize the quench point shown in the above figure and derives its meaning from the measurements made on short samples of the conductor in a test rig where various current densities, field strengths and temperatures can be applied. The figure also indicates that the operating field could be increased by lowering the temperature to 1.8 K, a solution that was chosen at the LHC.

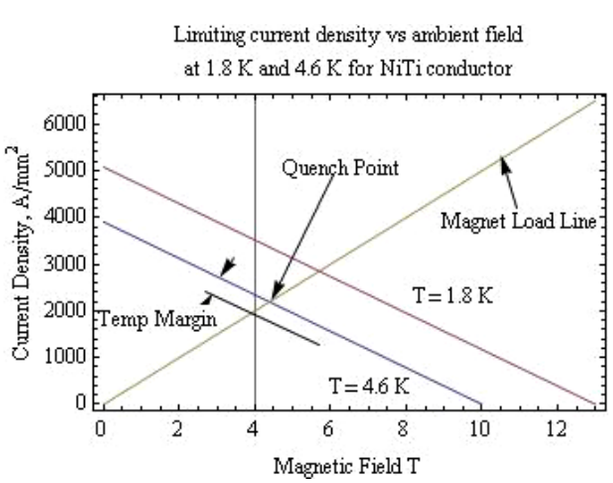

Fig. 2. Critical current for Nb–Ti at two temperatures versus the ambient field. The magnet load line is determined by the magnet design and is the high field point in the winding versus the winding current density.

2.1.1. *Superconductor cable development*

One of the great success stories for the HEP community was the commercialization of Type II superconductor alloys into useful cable [7, 8]. The collaboration of magnet builders, materials scientists and industry produced a spectacular advance. The graph in Fig. 3 shows in a grossly oversimplified manner the conditions that must be met. The alloy we will be concerned with is 46.5% wt Nb–Ti alloy. However, to make a useful conductor this material must be in filamentary form and surrounded by copper. Figure 3 shows a 0.5 mm copper strand with over 2000 imbedded Nb–Ti filaments that have a diameter of about 8 μm.

There are several reasons for this structure [4]. The first is that in a Type II superconductor, the flux penetrates the filament in small jumps as the field is increased. These flux jumps release a small amount of heat. The copper carries this heat away and keeps the filament below the transition temperature. If the filament should pass into the normal state, its resistance is very high and the joule heating will start to

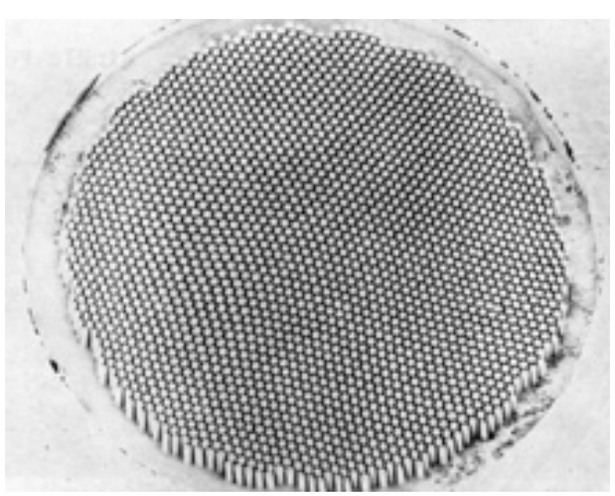

Fig. 3. Photomicrograph of a 0.5 mm strand. The copper has been etched away to show the individual Nb–Ti filaments. This strand will carry about 200 A at 4.6 K in a field of 4 T.

turn the whole strand normal and unless the current is turned off the strand will destroy itself. The second reason for the copper is to provide an excellent conductor for the current should the strand start to go normal. The copper used is very pure and at low temperature has only 1% of its room temperature resistance and can carry the full current long enough for protective action to be taken.

The strand is produced from rods of Nb–Ti about 3 mm in diameter and 65 cm long. Wilson originally purchased enough alloy for 1/6 of the ring and had it formed into these rods by (Teledyne) Wah Chang. This material was then distributed to manufacturers of superconducting strands, where it was loaded into hexagonal copper rods with a 3 mm coaxial hole. Next, 2000 of these rods were loaded into a close-packed array in an $\sim$250-mm-diameter copper cylinder and extruded under heat and high pressure into a cylinder $\sim$75 mm in diameter. At this point the cylinder was heat-treated and drawn down into the 0.5 mm strands. The exact details of this industrial process had large effects on the ultimate current-carrying capacity of the strand. There was intense competition among the participating companies to produce the best results and win the largest orders.

But the strand is still not suitable for use in a magnet because the magnet must be pulsed for use in an accelerator and the energy stored in it may exceed 1 MJ. In order for this to happen in tens of seconds, the inductance of the magnet must be kept low, which implies a small number of turns, which in turn requires very large currents. Thus in the Tevatron the conductor must carry about 4000 A, which requires 23 of the strands shown in Fig. 3. But this causes more problems.

Consider two of the strands in the cable that are necessarily joined tightly at the ends. If there is a net flux linkage in this loop when the magnet is pulsed, a large loop current will flow and the strands will not share the cable current equally. And a variation on this theme is seen within the strand where there can be loops enclosing flux between the filaments themselves. This latter problem was solved by twisting the strand through 360° every few inches during fabrication. The first problem was solved using an idea originated at Rutherford Lab [4]. This cable can be visualized by considering the 23 strands as being wound in a helix around a small coaxial cylinder and then flattening the resulting cylinder into a flat ribbon cable, as shown in Fig. 4. Magnets made with this cable showed large heat loads due to the eddy currents flowing through the loops generated by the top and bottom strands crossing each other. This problem was empirically fixed by coating every other strand with copper oxide, which is an insulator, and that effectively broke open the loops. Finally, as the cable must be positioned around a cylinder, as can be seen from Fig. 4, it is processed through a rolling mill that forms its cross section into a trapezoid.

The cable is next spiral-wrapped with an overlapping film of 25-μm-thick Kapton to provide electrical insulation. Finally, there is a spiral wrap of epoxy-impregnated glass cloth tape that when the coil is wound and cured holds the mass together (see Fig. 4).

The development of a successful conductor was a major accomplishment and was carried out by a close collaboration between Fermilab and the other national labs, materials scientists and industry. The initial purchase of a large amount of alloy allowed the distribution of identical raw materials to industry for the exploration and optimization of the many parameters that affect the ultimate current density and stability of the finished conductor.

2.1.2. *Fabrication of the coil package*

The coil is wound on a form and then placed in a precision mold and heated under high pressure to cure

Fig. 4. The cable developed for the Superconducting Super Collider, showing the epoxy-impregnated glass tape, the Kapton insulation and the filaments that have been exposed by etching.

the epoxy and produce an object that can be handled easily. Here again there was much to be learned. As we shall see, the dimensions of the coil had to be controlled to about 0.025 mm in order to produce the correct field and to keep the conductors from moving under the large magnet forces present during excitation.

Originally the mold was machined out of a solid piece of steel the length of the magnet. This was possible but slow for the ∼300-mm-long model magnets, and challenged the available machines to maintain a high accuracy over a length of ∼7 m. This led to the invention of laminated tooling, which was a major innovation [9]. The requirements on the coil are that its local cross section be the same over the length of the magnet. It turns out that industry has a well-developed capacity to make precision stampings out of sheet stock. And, even better, industry can quickly produce the dies necessary for stamping to an accuracy of a few μm. Thus, by forming the mold from steel stampings and stacking them together on a precision flat bed, one can produce a very accurate mold quickly and change it if necessary. Figure 5 shows such a mold with the hydraulic press in the rear.

The fabrication of the coils required a lot of research and trial. Too much epoxy could completely seal off access for the liquid helium cooling. The tolerance on the Kapton film thickness and the glass tape had to be carefully monitored to prevent the accumulation of changes in their dimension from causing large changes in the coil package dimensions.

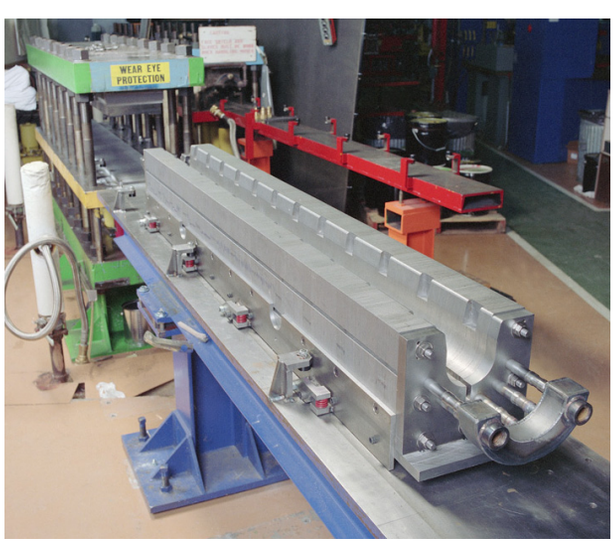

Fig. 5. A mold section made from lamination. The coil fits in the bottom and a second piece of the mold comes down from above. The pipes carry hot liquid to heat the mold and cure the epoxy.

2.1.3. *Constraining the forces*

Constraining the forces and maintaining the geometry of the coil package were two central problems that had to be solved when making a transition away from normal iron magnets, where the iron controls the field shape. The Tevatron coil has a 76.2 mm diameter and the magnetic field pressure in the bore is about 600 N/cm^2. A 1 m length of cable in the median plane of the coil package has a force of about 16,000 N forcing it outward. In addition, as can be seen from Fig. 1, the cable near the poles exerts a large azimuthal force that tends to compress the winding toward the median plane. The azimuthal force decreases to zero at the median plane, but the sum of all of the turns is large. The question of field accuracy will be discussed later, but the result of calculations shows that changes of any of the dimensions should be constrained to the order of 0.025 mm.

Early in the program, a novel method for containing the forces was tried. The coils were assembled on a series of spaced-out titanium rings and then overwrapped with stainless banding. There were two layers of banding under high tension wrapped in opposite directions to balance the torque. Figure 6 shows a one-foot model magnet using this technology.

It was soon found that the structure was not rigid enough to contain the forces, and the technique was abandoned. During the early part of the program many experiments were made on short magnets which could be quickly constructed and tested in an open cryostat filled with liquid helium.

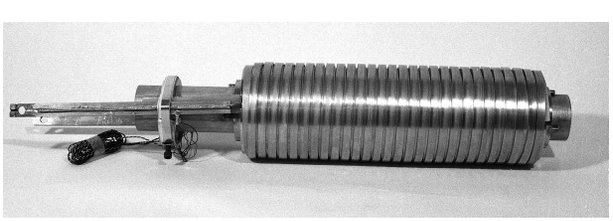

Fig. 6. A very early one-foot model magnet using spiral-wound stainless steel banding in two oppositely wound layers.

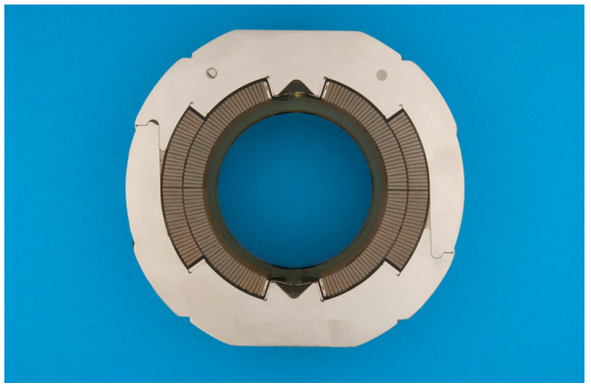

Fig. 7. A model magnet was constructed and, after testing, was sliced apart. This slice shows the details of the coil and stainless steel collars.

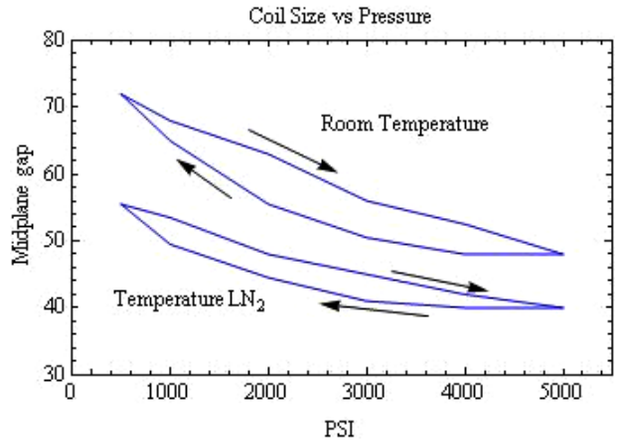

Fig. 8. Compressibility of the coil package at room temperature and at that of liquid nitrogen.

The solution found not only worked but has been an integral part of all subsequently constructed accelerator magnets. It was the original use of the technology mentioned above and shown in Fig. 5. Stainless steel stampings were made in a form that created a steel jacket around the outside of the coil.

The collars are split asymmetrically and the next layer down would have the joint between the two pieces reversed. The stainless steel is 1.5 mm thick and the layers are joined by axial welds along the outside. The whole package is later impregnated with epoxy to strengthen the structure. Additional rigidity is obtained by small dimples pressed into the steel that mesh with the underlying layer, and can be seen clearly near the top in Fig. 7.

The collars are first assembled into short packs, which are then placed around the coil package. The whole assembly is placed in a hydraulic press that closes the collars, and an automatic welding machine makes the axial welds along the outside that lock the structure together. There are two key points for maintaining the field accuracy. The first is that the collars must be thick enough to resist the tremendous horizontal force mentioned above. The second is a much more difficult problem to solve. The azimuthal force shown in Fig. 1 compresses the coil toward the midplane. Any motion of the coil boundaries is a disaster. The coil angles have been carefully chosen to make a uniform field and they are set by the collars, as can be seen in the above figure. As long as the coil stays in contact with the collar, the integrity of the field is assured.

So the key to the problem is to collar the coil with a press that compresses the coil package enough so that the elastic forces are always greater than any magnet force during excitation. A number of problems had to be solved and it was not clear that a solution existed. The main obstacle was that the coil, when cooled, shrank more than the stainless steel collars releasing some of the strain. Figure 8 shows the compressibility of the coil package at room temperature and at LN_2 temperature. This data was obtained by using a slice of a collared magnet, as shown in Fig. 7. The collars were cut along the midplane on one side, which released the collaring pressure. The force required to close the collar back to its original size gave a direct measure of the prestress in the package. The same measurement made at LN_2 temperature gave a measure of the force lost when the coil was cold. It was necessary that this force was great enough to ensure that the coil package didn't pull away from the collar during excitation.

One might think that the solution was to apply a high-enough collaring pressure to compensate for the differential shrinkage, but there was a limiting pressure that the insulation could stand before turn-to-turn shorts developed. The solution found involved very careful control of all of the dimensions, but would not have worked for higher field magnets, and alternative techniques have been developed and will be described later.

2.1.4. *Field errors*

This is an appropriate place to discuss the question of field errors. As mentioned before, since the field is primarily determined by the geometry of the

currents, any error in the coil shape will show up as deviations in the field. Since the bore is a current-free region, a harmonic expansion of the field can be made and the coefficients determined from the known current distribution. The information in the expansion is generally displayed as follows [5]:

$$B_y(x,y) = \mathrm{Re}\left[B_1 \sum_1^\infty (b_n + ia_n)\left(\frac{x+iy}{R_{\mathrm{ref}}}\right)^{n-1}\right],$$

$$B_x(x,y) = \mathrm{Im}\left[B_1 \sum_1^\infty (b_n + ia_n)\left(\frac{x+iy}{R_{\mathrm{ref}}}\right)^{n-1}\right].$$

It is customary to quote the value of the multipole fields at a radius $R_{\mathrm{ref}} \sim 2/3$ of the aperture divided by the central dipole value. Accelerators require that these error fields be of the order of 10^{-4} of the central bending field for stable beam behavior, and thus of the order of a few gauss. Therefore, both b_n and a_n are expressed in units, i.e. the actual value is multiplied by 10^4 to get a number of the order of 1.

The b_n are the so-called normal harmonics and are all driven by current distributions that are symmetrical between the top and bottom halves of the coil. The a_n are called the skew harmonics and are driven by left–right-symmetrical current distributions.

It is interesting to look at the Tevatron coil in Fig. 9 as a simple example. Assume that there is perfect right–left and top–bottom symmetry. Then all of the a's and all of the even b's are zero. It is easily shown in the case of "thin" coils, b_3 and b_5 can also be set to zero by adjusting the two coil angles. Thus the first term that comes into the expansion is the 14th pole, which varies like x^7, and evaluation of this term shows that it is negligibly small over the inner 2/3 of the aperture.

Table 2 gives the rms values measured for the 870 dipoles initially installed in the Tevatron [10, 11]. The data on the quadrupoles is available in Ref. 12 and a description of the measurement facility in Ref. 13. The values shown are integral values averaged over the length of the dipole. Control of the normal and skew quadrupole was the most difficult. However, it was possible to correct for an error in the coil by offsetting the center of the coil from the axis of the hole in the iron yoke, because the first effect of such an offset in the iron is to produce a small induced quadrupole. This correction will be described below.

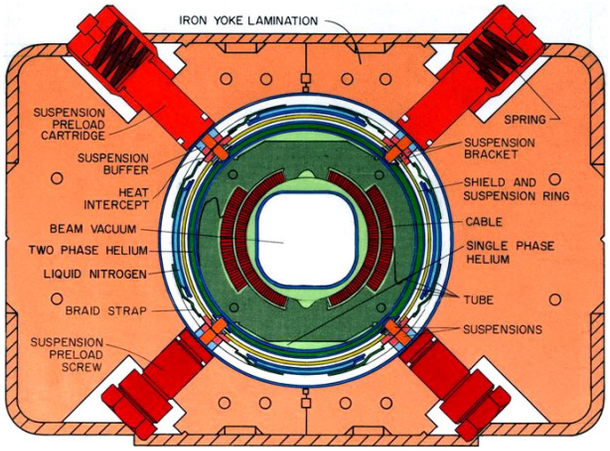

Fig. 9. Cross section of a Tevatron dipole.

Table 2. The rms values of the various multipole components of the Tevatron dipoles. The measurement was made at 4000 A. The coefficients are in units of 10^4 of the central field at a radius of 25.4 mm.

n	b_n	b_n	b_n	a_n	a_n
	Design	Mean	RMS	Mean	RMS
2		0.09	0.48	0.17	0.50
3	0.04	0.95	3.12	0.10	1.16
4		−0.23	0.77	−0.07	1.46
5	1.04	−0.57	1.32	−0.10	0.46
6		−0.07	0.32	−0.07	0.55
7	4.44	5.48	0.54	−0.07	0.29
8		0.04	0.17	0.22	0.26
9	−12.09	−12.52	0.33	−0.07	0.41
10		0.02	0.23	0.28	0.38
11	3.63	3.70	0.26	0.08	0.25
12		−0.01	0.20	−0.24	0.25
13	−0.82	−0.80	0.19	−0.05	0.22

There is a second systematic effect that must be corrected. The ends of the coil where the cable reverses direction cause a small change in the effective length of the magnet that varies like x^2, the same as the variation of the sextupole in the body of the coil. These two effects can be made to cancel. As the path moves off center the magnet becomes shorter, but the sextupole moment of the coil can increase the field so that the field integral through the dipole is constant.

2.1.5. *Persistent current effects*

Superconducting cable comes with a small problem in that it produces small systematic error fields. According to the Bean model [14], the currents that

flow are always at the critical limit and the total current is the sum of the transport current and the shielding current, which is trying to keep the flux from penetrating the metal. A cylindrical filament in a uniform field has an induced dipole moment due to the shielding currents, and since there are several million of these filaments in the winding, they can coherently produce a residual field that can lag the ambient field and produce an open loop magnetization curve. Since the windings are very nearly symmetrical, only the spatially symmetric normal harmonics are generated and their magnitude is of the order of tens of gauss, a magnitude that is negligible for the guide field but has big implications for the dynamics of the focused beam. The biggest effect comes from the sextupole moment which controls the chromaticity of the machine. If it were static, it could be easily compensated for by the correction elements in the machine.

However, the trouble comes because these persistent currents decay logarithmically from their dynamic value if the magnet excitation is suddenly held constant [15]. The magnet is cycled from injection to high field and then finally back to low field for another cycle, where it may remain for a long period while particles are injected. For the Tevatron, this can be of the order of 30 min as both the protons and the antiprotons must be injected. While injection is taking place, the persistent sextupole field decay is a relatively slow process, but it turns out that at the start of acceleration, the magnetic moment returns to its dynamic value ("snap-back") with only a very small change of field. This sudden change in chromaticity must be carefully corrected for stable operation.

The fact that there is an open loop means that there is also an energy loss when a magnet is cycled around a loop and this heat must be carried away by the cryogenic system [16]. Both the heating and the magnetization can be reduced by making the filament smaller in the conducting strand. In the Tevatron the filaments are about 8 μm in diameter and the hysteresis loss is about 200 J per magnet cycle.

3. The Tevatron Magnet Development

As indicated in the introduction, the development of the Tevatron was an experiment. Never before had over 1000 superconducting magnets been produced. Thus constructing a factory as part of the experiment was essential to the process of learning how to make magnets. There were two lines of attacking this problem. The first was to start a vigorous model program that was based on 300-mm-long model magnets. These could be produced rapidly; in some cases a model with a different parameter could be produced in a week. This program was the basis for understanding how to fabricate and insulate the coils and was also crucial for the cable development program.

At the same time tooling was being developed for full length magnets based on what was being learned from the model tests. In the end almost 200 full length coils were fabricated and tested before the actual construction of the machine began. Some of these magnets were later used in beam lines where the field quality was not so important. A crucial piece of this program involved the development of instrumentation that could measure the field of a coil package at room temperature [17]. After the coil was collared, it was taken to a measurement stand where a full length probe consisting of a set of parallel stretched wires was inserted. The coil was excited with a 10 A sinusoidal wave form. A phase-locked voltage integrator measured the flux through the parallel loops and derived the multipoles. The system was able to monitor the lower harmonics up through the sextupole terms and was thus able to close a feedback loop around the factory. If the field components started to drift, the cause could be looked for and corrected. But, more important, systematic effects due to small systematic changes in the components could be corrected by placing small shims to slightly change the angle subtended by the coils. This measurement was very cost-effective, in that it insured that a coil placed in a cryostat and yoke at considerable cost and labor would not have serious defects when it was measured as a completed package.

3.1. *The cryostat and yoke*

A cross section of the completed magnet is shown in Fig. 9. The yoke construction followed the normal procedure of using stamped iron laminations stacked together in two sections split symmetrically about the vertical center line [18]. The only special feature was that the magnets were long enough so that, if straight, the curve of the beam through

the magnet would have had a sagitta of 5 mm consuming ±2.5 mm of aperture. This problem was successfully solved by curving the yoke and forcing the cryostat and coil, which were constructed as straight elements, into the curved cavity. Welds were then made to lock the structure in place.

The cryostat must fit in the space between the outside of the collars and the inside of the iron yoke. The iron is at room temperature — a real challenge and an ingenious piece of engineering!

The main part of the cryostat comprises three stainless cylinders consisting of the beam tube and two closely spaced cylinders around the outside of the collars. The region between the beam tube and the first stainless cylinder is filled with liquid helium under pressure and forms the supply pipe. After going through a string of eight magnets, it expands through a Joule–Thomson valve and passes back along the string in a space between the first and second stainless steel cylinders. It is in intimate contact with the inner volume and absorbs heat from the coil assembly, boils, and passes back to the liquefier as a two-phase liquid. This keeps the inner coil at almost a constant temperature. There is an intermediate shield and then a liquid nitrogen shield before coming to the outside cylinder which closes off the cryostat insulating vacuum.

We will leave the cryogenics system [19] here, but one should appreciate the tremendous success of these enormously dispersed systems. An obvious challenge was making the thousands of leak tight welds necessary to form the cryostat and the difficulty of leak-checking the completed system. The LHC was an even bigger challenge.

3.2. *The coil support system*

The Tevatron had to solve one problem that was not pertinent to later machines. Since the iron was warm, there had to be a coil support system devised that had limited heat leak and yet held the coil package firmly in place. When the coil is cooled it shrinks both axially and radially. It is firmly anchored in the axial direction at its center. There are nine support points along the axis and the ones on either side of the center must allow for axial slipping.

However, more troublesome is the shrinkage in the radial direction, which is almost 1 mm. As can be seen in Fig. 9, each of the nine stations has four support pillars at 45° which are points on the collars that do not change radius as the coil is excited and becomes slightly elliptical. The bottom two are fixed at a position that will center the cold coil properly, but are also adjustable. The top two are spring-loaded and allow motion of the support point as the coil is cooled. The springs must be strong enough so that if the coil moves off center their restoring force is larger than the magnetic force, pulling the coil in the direction it is offset.

It turned out to be very useful to be able to move the coil slightly off center, because that allowed the correction of the intrinsic quadrupole errors in the coil package. The induced field from the iron due to an offset coil is a quadrupole whose strength is proportional to the offset. Each magnet was measured cold in the Magnet Test Facility, and quadrupole error field was determined. Shims were then placed under the external bolts that shifted the coil package by an amount to set the total moment to zero.

3.3. *Quench protection*

A superconducting magnet is intrinsically unstable. If some piece of the conductor is forced into the normal state, the subsequent joule heating may drive more of the conductor normal and the normal zone will propagate. Consider a small length, δz, receiving a small pulse of heat that is sufficient to drive it into the normal state. The current will immediately transfer to the copper, which has about 1% of its room temperature resistivity. If δz is sufficiently small, the heat capacity of the surrounding medium may be enough to overcome the joule heating in the copper, and the cable returns to the superconducting state. However, the magnet is most vulnerable when it is at full field and operating very near its upper limit, and there will be some δz that is long enough so that the joule heating will overcome the cooling and the quench wave will propagate along the cable with a velocity between 1 and 10 m per second. As more of the cable heats up, it will heat adjacent turns and the quench will propagate through the winding. If the current is not turned off, the cable will destroy itself and the insulation.

To calculate the limits that must be met, consider the following expression for the increase in temperature of a small section of cable with resistance $R(T)$ and heat capacity $c_p(T)$ and carrying a

current $i(t)$:

$$dT = \frac{i(t)^2 R(T) dt}{c_p(T)}.$$

Collecting the temperature-varying terms together, we can write

$$\int_0^t i^2(t) dt = \int_{T_1}^{T_2} \frac{c_p(T) dT}{R(T)}.$$

The right hand side can be evaluated. The resistance is essentially determined by the copper, which is very pure and cold at the start. The heat capacity is small for the metal because initially it is at low T where the heat capacity varies as the third power of T, but the liquid helium contained in the strands provides the large initial heat sink. T_2 is the upper temperature that the coil will survive. Putting in these numbers, one obtains a limit for the integral over time of the square of the current. For the Tevatron this number was of the order of 7×10^6 A^2s for a temperature increase to about 200°C, and exceeding 12×10^6 A^2s will damage the conductor. Since the magnet current is of the order of 4000 A, something must be done in a fraction of 1 s if the magnet is not to destroy itself.

A Tevatron magnet contains about 300 kJ and it is not practical to extract this energy in a short time. The solution was to short the offending magnet which bypasses the bus current around it and at the same time turn the whole magnet normal and absorb the energy in the magnet as heat in the whole winding, which then contains the temperature increase to reasonable values [20]. In the meantime, the energy from the rest of the machine is extracted in the normal manner.

The solution involved building into the magnet some stainless steel foils that acted as heaters. When a quench was detected, a capacitor was discharged into the foils, which provided heat to a large section of the coil package and which spread the quench uniformly throughout the winding.

The signal to detect a quenching magnet is the resistive voltage developed across the normal zone. We will not discuss this more here, but the quench detection and protection system represents a major portion of the control system.

A quench of an accelerator magnet system is a violent event. Not only must the magnets be protected electrically, but there are also very large mechanical forces due to the very rapid vaporization of the liquid helium. This requires very careful design of the cryostat to survive these events without opening up leaks in the myriad of welds, as well as a gas-handling system that minimizes the loss of helium.

3.4. *Progress at other machines*

The first operation of the Tevatron was on July 7, 1983, when it accelerated beam to 512 GeV [5]. Subsequently it has been used in both the fixed target mode and as a pbar-p collider for almost 25 years. The above description outlines the problems that were solved and indeed the cross section of any of the subsequent accelerator magnets shows the heritage of this early work. It is interesting to examine some of the initial choices that were made. For instance, the decision to keep the iron warm had a major influence on the magnet design. The Tevatron covered a larger area than any existing cryogenic installation, and cooling both the coil and the iron yoke would have needed either an enormous plant or a very long time. There was great concern that if the magnets were not reliable and required replacement, the downtime would not be acceptable. Early operational experience verified that this was a wise decision, as many changes and corrections were necessary. However, the experience now is that perhaps one magnet a year needs replacement and the time to replace a magnet and resume operation has turned out to be about one week. The big advantage of having cold iron is that it can help support the large magnetic forces within the magnet. HERA [21] was the first to take advantage of this, and the reliability of superconducting magnets has been quite sufficient to justify this choice in the design. The HERA magnets were also longer, 8.824 m vs. 6.4 m, and worked at a higher field, 4.68 T vs. 4 T, for the Tevatron.

An additional advance at HERA was the use of aluminum collars. It was known at the time the Tevatron magnets were being developed that the loss of compression in the collared coil due to the greater thermal contraction of the coil compared to the stainless steel collars could be alleviated by using aluminum collars. HERA developed an elegant system for controlling this differential contraction. An additional improvement was to use spacers within the coil block to enhance the approximation to a $\cos\theta$

current distribution and reduce the lower harmonics in the field.

Finally, HERA was the first to have the magnets produced industrially. This involved transferring the design to industry and carefully monitoring the product through the production cycle [22]. The construction started in 1984 and was operational in 1990.

During the period from 1985 to 1995 there was a great deal of intense work on superconducting magnets at other locations. The Relativistic Heavy Ion Collider (RHIC), at Brookhaven National Laboratory, developed a very simple single-shell coil that used the iron collars directly to contain the winding.

A big challenge for this magnet was careful control of the iron properties and the successful modeling and control of the effects of saturation on the field quality. It was the first magnet that employed saturated iron in the yoke [23].

The Superconducting Super Collider (SSC) story is a modern tragedy, but it did involve all of the US national laboratories in the magnet development program, and the technology of magnet construction was refined. However, the present state of the art is exemplified by the LHC, which has successfully overcome the complex mechanical problem of having two magnets in one yoke and cryostat while increasing the field up to 8.3 T. In addition, the fields in the two apertures must track each other precisely in magnitude and shape from injection at 450 GeV, where the persistent currents generate a large sextupole to 7 TeV, where loss of beam can cause enormous damage to the machine. Another bold innovation is the use of superfluid helium for cooling the magnets. A detailed description of the magnet production gives an excellent overview of the present state of the technology.

4. The Main Dipole in the Large Hadron Collider

4.1. *Design*

The development of models to prove the feasibility of superconducting dipoles with a 10 T magnetic field, i.e. significantly higher than that obtained in previous accelerators magnets, started nearly 20 years ago [24]. These field values could be achieved either by lowering the operational temperature of the Nb–Ti to around 2 K, or by using a material with a larger critical field and critical current, such as Nb_3Sn [25]. Lowering the operational temperature of the Nb–Ti had the disadvantage of making the magnet more sensitive to any heat deposition in the coil, either from the beam or from the magnet itself (mechanical movements, flux jumps). On the other hand, Nb_3Sn presented worse mechanical properties, strain sensitivity, difficulties in manufacturing and, last but not least for such a large project, higher costs. At the beginning of the 1990s, the Nb–Ti option was retained.

Nearly 10 years of short models and long prototypes (10–15 m) resulted in three generations of dipoles. The first one [26] was based on a two-layer coil with 17-mm-width cable, aluminum collars, a 10 m length and a 50 mm aperture. In the second one the length and the aperture were increased to 15 m and to 56 mm respectively, the cable width was reduced to 15 mm, and the cryogenic line was placed outside the dipole cryostat [27]. In the third generation, the collar material has been changed to stainless steel, with a revised yoke design that gives better support and with a gap between the two iron yoke halves that is closed at room temperature [28].

In the final design, the LHC dipole has a short sample field of 9.7 T and an operational field of 8.3 T in a 56 mm aperture bore using Nb–Ti cables cooled at 1.9 K [28, 29]. Compared to the previous accelerator dipoles, the LHC cable has a larger width (∼15 mm), and a larger strand diameter of the inner cable (∼ 1 mm; see Fig. 10).

The main strand parameters are listed in Table 3. The critical current specifications are given at 1.9 K, and correspond to having a current density in the superconductor of $\sim 2100\,\mathrm{A/mm^2}$ at 9 T or $\sim 1500\,\mathrm{A/mm^2}$ at 10 T. These current densities are about 30% larger with respect to that specified 25 years earlier for the Tevatron magnets [30].

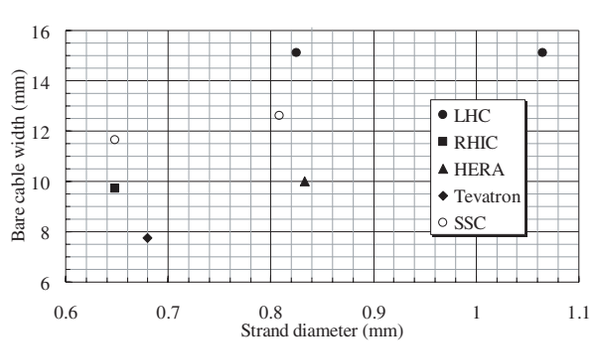

Fig. 10. Strand diameter and cable width used in five dipoles.

Table 3. Main parameters of the LHC dipole strand.

	Inner	Outer
Filament diameter (mm)	0.007	0.006
Number of filaments	~ 8900	~ 6500
Strand diameter (mm)	1.065 ± 0.0025	0.825 ± 0.0025
Copper–noncopper ratio	1.65 ± 0.05	1.95 ± 0.05
Critical current (A) at 10 T	≥ 515	
Critical current (A) at 9 T		≥ 380
RRR	≥ 150	≥ 150

Table 4. Main parameters of the LHC dipole cable.

	Inner	Outer
Number of strands	28	36
Mid-thickness (mm) at 50 MPa	1.900 ± 0.006	1.480 ± 0.006
Keystone angle (°)	1.25 ± 0.05	0.90 ± 0.05
Transposition pitch (mm)	115 ± 5	100 ± 5
MIITS [300 K] (MA^2s)	45 [8 T]	30 [6 T]
Critical current (A) at 10 T	≥ 13750	
Critical current (A) at 9 T		≥ 12960
Interstrand cc resistance ($\mu\Omega$)	≥ 15	≥ 40
RRR	≥ 70	≥ 70

The cable parameters are summarized in Table 4; the values for the critical current correspond to assuming 5% degradation of the strand performance.

The cable insulation is made up of two polymide layers 50.8 μm thick, with 50% superposition, plus a third adhesive layer 68.6 μm thick wrapped in such a way that it leaves a 2 mm gap to ease the superfluid helium penetration between cable turns. The polymide aims at withstanding a turn-to-turn voltage of around 100 V [31].

After some iterations on the coil design, a six-block, two-layer $\cos\theta$ layout was selected [32], not far from the SSC dipole layout, with an $\sim 10\%$ larger aperture and $\sim 20\%$ larger cable (see Fig. 11). Due to the large coil width and collar width, the iron contribution to the field at the operational current is limited to 18% (25% in the Tevatron dipoles and 57% in the RHIC dipoles). Notwithstanding the large field, iron saturation in the LHC dipoles is much less critical than in the RHIC dipoles: at collision energy, it decreases the transfer function by about 0.6% in the LHC dipoles, and ten times more (7%) in the RHIC dipoles. This is due to the fact that in the LHC dipoles both the coil and the collars are very thick, and therefore the iron is far from the aperture.

The iron also has a limited beneficial effect on the LHC dipole short sample field, increasing it by 3.5%. Multipoles up to b_{11} have been optimized [32]

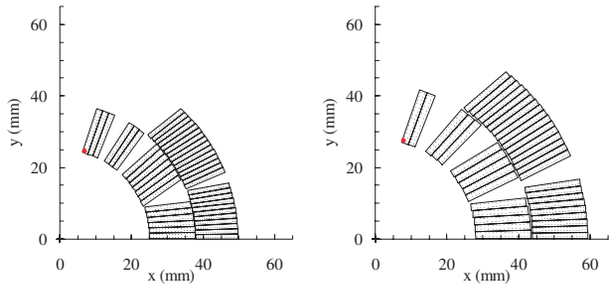

Fig. 11. Coil layouts of the SSC (left) and the LHC (right) main dipole.

at the level of $\sim 10^{-4}$ times the main component (i.e. one unit).

The curing cycle of the coils reaches a maximum temperature of 190°C and a maximum pressure of 100 MPa, for a few hours [33]. The curing is used to activate the glue of the third insulation layer and to give the correct dimensions to the coil. The cables from the two layers are joined with a ramp splice and the coils are powered in series; since the outer cable is smaller, this provides a larger current density in the outer layer of 23% (it was 30% in the SSC dipoles). The larger cable width, the improved cable properties, and (especially) the lower operational temperature (1.9 K instead of 4.2 K) allow the LHC dipoles to reach the unprecedented short sample field of 9.7 T and an operational field of 8.3 T, i.e. 86% of the short sample limit (inner-outer layer) (see Figs. 12 and 13), and with a temperature margin of 1.5–1.6 K (inner/outer layer).

The electromagnetic forces acting in the azimuthal direction on the coil mid-plane at 8.3 T are ~ 450 kN/m, corresponding to a stress of ~ 60 MPa.

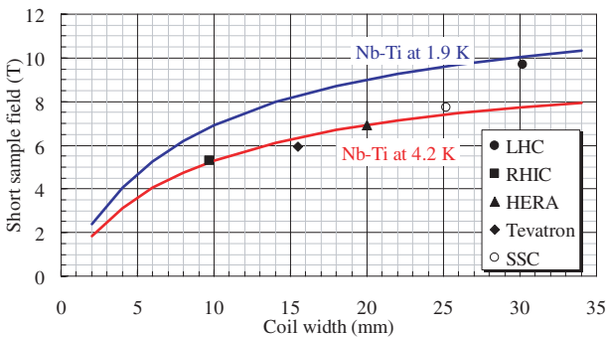

Fig. 12. Short sample field versus coil width for five dipoles (markers), and estimate for an ironless $\cos\theta$ coil with a 0.3 filling factor. The same Nb–Ti cable properties have been assumed for all dipoles.

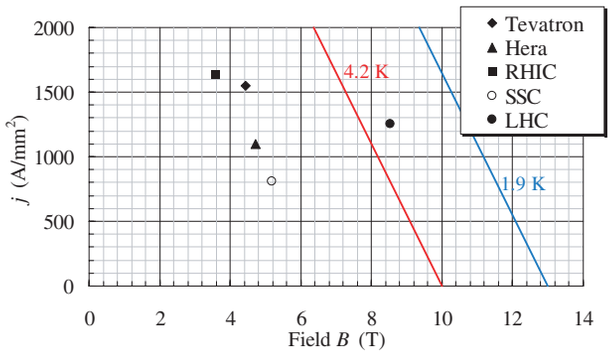

Fig. 13. Operational values of current density in the superconductor and magnetic field in the bore for five dipoles (markers), and typical values of the critical surface of Nb–Ti at 4.2 K (red line) and at 1.9 K (blue line).

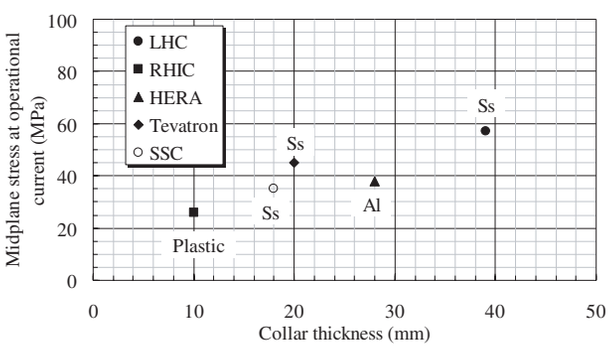

Fig. 14. Average stress in the mid-plane in operational conditions versus collar thickness and material for five dipoles.

This stress is 30% larger than what was reached in the Tevatron dipoles (see Fig. 14, where the collar material is also reported). We point out that whereas larger forces can always be contained by an appropriate mechanical structure, large stresses induce strain in the coil which can give an ultimate limit to performance. For this reason we believe that a comparison of the mechanical challenges in superconducting magnets should be given in terms of stress and not of force.

The LHC accelerates and collides two counter-rotating proton beams. Contrary to the SSC, where one had two separate single-aperture dipoles, in the LHC a two-in-one dipole concept was developed: the two apertures share the same cryostat and the iron shielding to fit the limited space available in the tunnel. During the dipole prototype phase, both separate collar [24] and twin collar [26] options were considered. The final design [28, 29] presents a twin

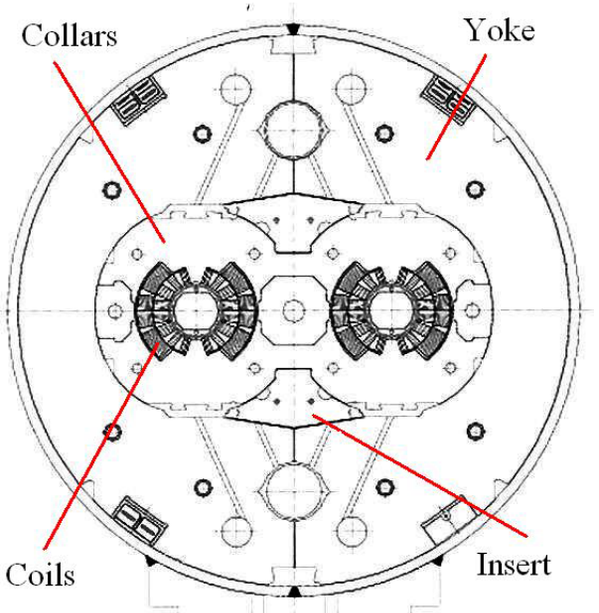

Fig. 15. Cross-section of the LHC dipole cold mass.

stainless steel collar structure retaining both apertures in a common yoke (see Fig. 15). This option was taken to save costs, under the correct assumption that the resulting mechanical and magnetic coupling between the apertures would not have affected the performance. The large thickness of the collars (40 mm; see Figs. 14 and 15) is due to a design originally foreseen for aluminum collars; the switch to stainless steel collars was carried out in the final phase of the full-size prototypes [34]. As a result, the collars bear most of the electromagnetic forces at nominal field.

Collars are made up of 3-mm-thick laminations and with stringent specification on the permeability. Nevertheless, their protrusions (which are usually called "noses") give a nonnegligible contribution to the field quality, which is compensated for via the coil geometry. It is made up of 5.8-mm-thick low-carbon-steel laminations. It is vertically split and the two halves are in contact (closed gap) both after assembly and after cool-down. Forces are transmitted from the yoke to the two-in-one collars also through an inclined iron insert (see Fig. 15).

During the assembly one usually aims at reaching a sufficient coil compression (prestress) to avoid coil movements in operational conditions. For the LHC dipoles, the target prestress at room temperature after collaring was fixed at 70–75 MPa

[33]. Collars are locked using rods, which results in a large spring back after collaring ($\sim 60\%$). For this reason the prestress needed during collaring is ~ 130 MPa; during the model and prototype phase it was carefully verified that the insulation could withstand these large pressures.

During the cool-down, the low thermal contraction of the stainless steel collars coupled with the large thermal contraction of the superconducting coils contributes to a significant prestress loss (see Fig. 16), similarly to what was found for the SSC dipoles [35]: the final target for the azimuthal stress at 1.9 K is ~ 30 MPa. The mechanism of the prestress loss is due not only to the differential thermal contraction but also to the hysteresis in the mechanical behavior of the coil [36]. Short models and prototypes were instrumented with capacitive gauges to measure the prestress level in the coil [37]. Short models having an unloaded coil at full energy did not show worse quench performances [38], and even though the series magnets had no capacitive gauges, there is evidence that part of the LHC dipoles have unloaded coils at full energy. The minimal required level of stress in superconducting magnets is still an open issue in the literature.

The sensitivity of the prestress on the azimuthal coil size has been measured with dedicated experiments [39]; a 0.1 mm larger coil gives a larger stress of ~ 12 MPa at room temperature and of ~ 6 MPa at 1.9 K. The tolerance on the prestress at room temperature after assembly has been set at ± 15 MPa, thus giving a ± 0.12 mm window on the coil size. Pole shims of variable thickness have been foreseen [33] to keep the prestress under control in the case of coil sizes outside tolerances.

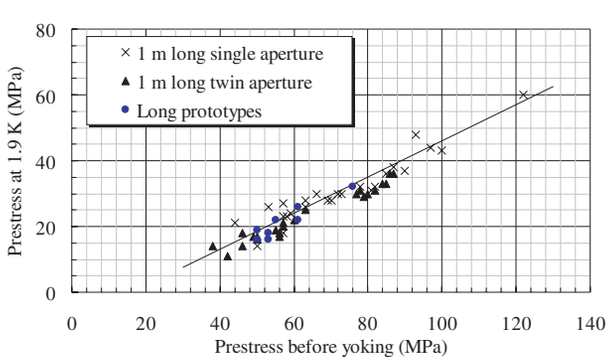

Fig. 16. Azimuthal prestress at room temperature after assembly versus azimuthal prestress at 1.9 K measured for LHC dipole short models and prototypes.

The collared coil and the yoke laminations are enclosed by a shrinking cylinder welded with 150 MPa circumferential stress. The welding also imposes the desired curvature on the cold mass, which corresponds to a nominal sagitta of 9.14 mm [40]. The main parameters and performance of the cold mass are given in Table 5 and compared to Tevatron, HERA and RHIC dipoles.

The cold mass (coil, collars, laminations and shrinking cylinder) contains a static bath of helium II at atmospheric pressure. The iron yoke laminations contain the heat exchanger tube, which extracts the heat during the operation at 1.9 K and during cooling from 4.2 to 1.9 K. It is a seamless, round, oxygen-free copper tube with an outside diameter of 58 mm, and a thickness of 2 mm. In operation it carries a two-phase flow of saturated superfluid helium at 16 mbar [41]. The helium is provided by an external cryogenic distribution line (QRL) which runs parallel to the magnets. The line contains the helium in different thermodynamic states which are used for intercepting the applied heat loads at a higher temperature, thus saving the cost of refrigeration of the whole machine [41]. In the arcs, the QRL feeds the machine through the main quadrupoles. Temperature levels range from shields at ~ 70 K in the cryostat, to ~ 20 K for the cooling of the beam screen, to 1.9 K for the main dipole cold masses.

The cryostat is a low carbon steel cylindrical vacuum vessel of 914 mm diameter [42]. The cold mass lies on three support posts made of glass fiber-reinforced epoxy, with two heat-intercepting plates at 4–10 K and 50–65 K. According to the design, the posts at the extremities are free to move longitudinally, and the central one is free to move radially;

Table 5. Parameters of four superconducting dipoles; field, current, inductance and energy are given at nominal values (collision energy).

	LHC	Tevatron	HERA	RHIC
Field (T)	8.3	4.3	4.7	3.5
Current (kA)	11.8	4.3	5.0	5.05
Inductance (mH)	98.7	32	58	28
Energy (MJ)	6.93	0.30	0.73	0.35
Magnetic length (m)	14.3	6.4	8.8	9.45
Cold mass weight (t)	27.5	NA	NA	3.6
Nominal/injection field	15.5	6.5	20.3	8.62
Temperature (K)	1.9	4.2	4.5	4.3–4.6
Coil diameter (mm)	56	76	75	80
Number	1276	774	416	264

this has been done to avoid stress on the post during cool down and warm-up. During the production, it has been decided to block the central post to better control the dipole shape [43]. Contrary to the case of the RHIC dipoles, there was no need to use external welding on the cold mass to control the dipole shape.

As in the HERA machine, dipoles are equipped with correctors to compensate for sextupole, octupole and decapole components. Sextupolar correctors (usually called "spool pieces" in the specialized literature) are mounted on each dipole, whereas octupolar and decapolar correctors are mounted every second dipole.

The machine is divided into octants which are individually powered, i.e. 154 dipoles are powered in series. The dipole protection is ensured by quench heaters placed between the outer layer and the collars. The firing time after quench detection is of the order of 20 ms, which assures that the temperature of the hottest spot is less than 300 K. Each dipole is equipped with a cold diode that during a quench bypasses the high current (up to 12 kA) with a decay time of around 100 s [42].

4.2. *Production and quality control of components and assembly*

For such a large project as the LHC, cost is a major issue and costs relative to the magnetic system are strongly related not only to raw material price, but also to tolerances on components and assembly procedures. LHC large production offered a unique opportunity to judge the soundness of the required tolerances with good statistics. Here we will briefly review the main results, showing that in most cases the tolerances were not far from what was just needed. The other important aspect is that one faulty magnet is enough for the LHC not to work. For this reason, the techniques for the quality control and test are extremely important, since one has to avoid having even a single faulty magnet installed in the ring. In this section we will also review the strategies used in the quality control of such a large production.

The cable production was shared between two manufacturers for the inner layer and five for the outer layer. The cable critical current was measured on a sample of $\sim 25\%$ (see Fig. 17). The specifications on critical current have been met, and average values $\sim 10\%$ larger than specification have been obtained [45]. Some outliers as shown in Fig. 17 have been

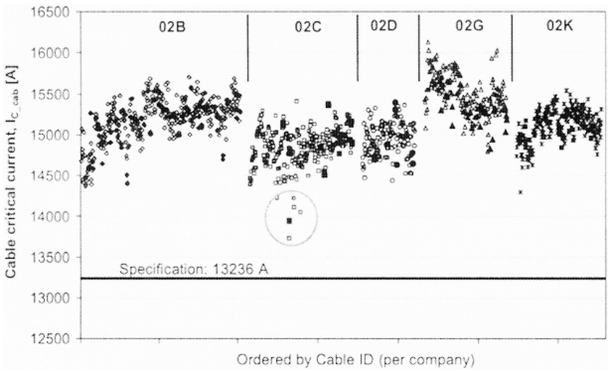

Fig. 17. Critical current measurements of the outer layer cable [45].

traced back to production features. The specification required the absence of cold welds within the length of superconducting cable used for winding each pole. During the production, a bunch of cold welds localized in the same section of the cable, and limiting the dipole performance to 60% of the short sample limit, were found in one case.

The field quality at injection is affected by the persistent currents in the cable. To monitor this effect, the magnetization of the strands was measured. A hysteresis cycle up to 1 T is performed, and the width of the loop at 0.5 T has to meet specification (30 and 23 mT for the outer and the inner layer, respectively) within 4.5% [46]. In order to meet this goal, strands with extreme values of magnetization were sorted during cabling. For the inner layer, an $\sim 13\%$ difference in the magnetization between the two producers was found; this was traced back to manufacturing procedures, and its impact on the performance was judged as acceptable. Notwithstanding the large number of manufacturers, a good homogeneity of the global production was obtained. This allowed the mixing of cable from different manufacturers in the same octant, contrary to the original baseline of the installation scheme (see also Subsec. 4.5). The measured cable dimension has been within the tight tolerances of ± 0.006 mm (see Fig. 18).

Three manufacturers (Alstom, Ansaldo Superconduttori and Babcock-Noell) have assembled the 1232 dipole cold masses plus 46 spares. The production steps involved the coil winding and curing, the assembly of collars and the collaring, the assembly of the iron yoke and the welding of the shrinking cylinder. The initial plan foresaw each octant to

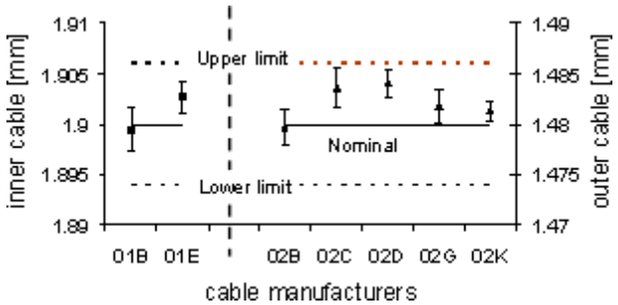

Fig. 18. Dimension of the cable during the production.

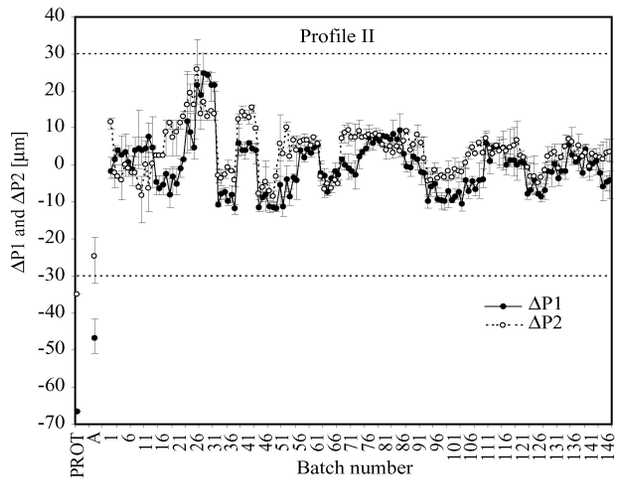

Fig. 19. Dimension of the copper wedge II along the production (difference with respect to nominal values), and two batches used at the beginning of the production.

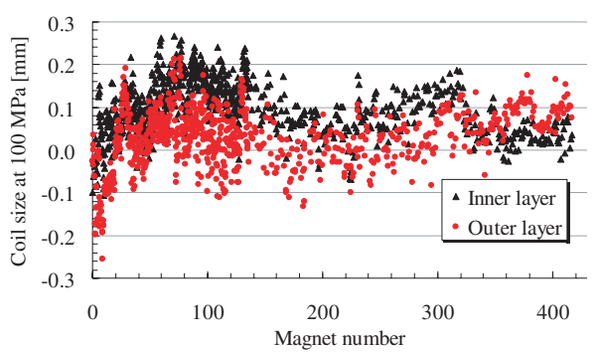

Fig. 20. Measured azimuthal coil size (difference with respect to nominal values, average left–right) in one of the dipole manufacturers.

be produced by the same manufacturer; after the results of the first magnetic measurements, showing a remarkable homogeneity between the firms (see Subsec. 4.3), this scheme was abandoned and one third of the production was allocated to each manufacturer.

Copper wedges of 3.6 m length were produced by Outokumpu. Approximately 1% of the production has undergone several types of tests: physical and chemical tests, and dimensional tests. The transverse dimensions are critical for the correct position of the winding, i.e. for the field quality. The tight tolerance of ± 0.030 mm has been kept through all the production [47]. A negligible influence on the field quality has been observed. On the other hand, a batch out of tolerance by around 0.050 mm used in the early part of the production (see Fig. 19) has shown a visible impact on b_3 [47].

The azimuthal size of the coils was measured at 70 MPa in 25–50% of the production, depending on the cold mass assembler. The curing is instrumental in giving the correct size to the coils: note that the pile-up of the tolerances on the cable (± 0.006 mm) and on the polymide ($\pm 3\%$) would give a coil precision of ± 0.3–0.4 mm. The initial tolerance of ± 0.025 mm on the average coil size [33] has been shown to be not realistic: measured coil sizes [48] along the production are in general within ± 0.2 mm, and for most of the production within ± 0.1 mm (see Fig. 20 for the production in firm 1). This permitted using nominal pole shims for 94% of the whole production. Nonnominal shims of up to ± 0.1 mm have been used in 6% of the coils, and of up to ± 0.2 mm in four magnets; in this case, the expected change in the allowed harmonics $b_3, b_5, b_7, \ldots$ has been observed.

Stainless steel collars have been produced by two firms (5/8 by Malvestiti and 3/8 by FSG); tight tolerances of ± 0.020 to ± 0.030 mm (depending on the position in the profile) on the complicated two-in-one shape have been set. Approximately 0.07% of the collars (three per magnet) were measured in around 100 points for quality control. In general the collars have been found to be precise within ± 0.040 mm; the two manufacturers have shown similar dimensions. Despite the fact that the collars did not meet the original specifications, the impact on field quality has not been relevant [49]. Collar permeability was specified at 1.003 ± 0.002, and was kept all along the production.

Iron yoke laminations have been produced by two manufacturers. The tolerance on the stacking factor has been fixed to $98.50 \pm 0.25\%$; since the iron contributes about 18% of the magnetic field, this tolerance gives a window of ± 5 units on the transfer

function. The situation here is less critical than in the case of RHIC, where more than 50% of the field was due to the iron and a stricter control of the iron mass was required.

The cold mass shape has been established using a laser tracker Leica^{TM} [40]. The tight tolerances on the longitudinal shape have been fixed to ± 1 mm along the reference orbit, and to ± 0.3 mm at the end of the magnet, where the multipolar correctors (spool pieces) are located. This tighter tolerance on the ends has been set to avoid harmonics feed-down from the correctors, which could have been critical for the beam. The sagitta of the produced magnets has a mean of 9.4 ± 0.9 mm (one sigma), i.e. within the tolerances (see Fig. 21, left). Around 80 magnets from one of the assemblers have a systematic shift of the corrector position with respect to tolerances of about 0.4 mm; this nonconformity has been judged as acceptable for the beam dynamics (see Fig. 21, right).

All the information and tests relative to each cold mass have been stored in a Manufacturing Test Folder (MTF). Nonconformities that occured during the fabrication process have been recorded; when judged as not affecting the magnet performance, the anomaly has been registered and the assembly has been continued. On the other hand, when the nonconformity has been judged as nonacceptable (for instance a fault in the insulation), corrective actions have been taken. In each firm, two resident CERN inspectors followed the assembly, the documentation, and have provided the link to two CERN project engineers in charge of the production follow-up.

During the cold mass assembly, room temperature magnetic measurements were used as a diagnostic tool, as has been done for both the Tevatron [17] and RHIC [50]. Over the whole production, this

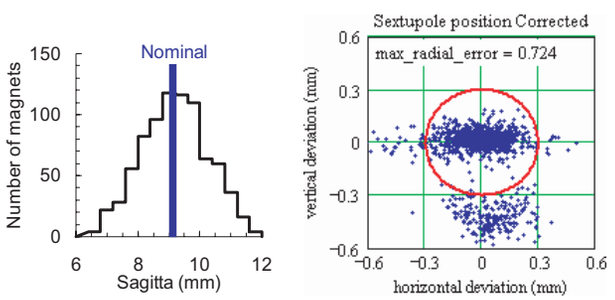

Fig. 21. Sagitta of the cold masses (left) and position of the correctors (right).

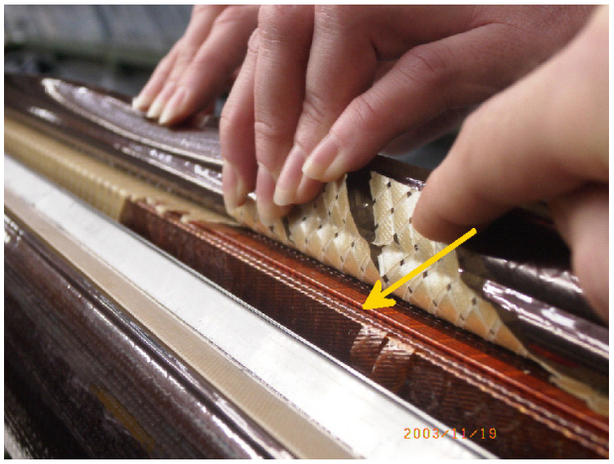

Fig. 22. A case of bad coil curing giving an inner radial movement of two turns of the inner layer, upper pole, of about 1 mm, found through anomalies in room temperature magnetic measurements.

technique allowed rescuing 19 faulty magnets (1.5% of the production) at the level of the collared coil: 5 wrong assembly cases (as double or a missing component), 2 wrong components, 8 cases of wrong procedure (a bad coil curing giving detachment of the last block of cables during collaring; see Fig. 22), and 4 other cases [51]. Magnetic measurements have also been used to successfully locate the position of electrical shorts during the assembly in 18 cases [52].

Thirty-one magnets (2.4% of the production) have been returned to the manufacturer and rebuilt after tests at 1.9 K at CERN: 14 of them for insufficient quench performance, 10 for electrical shorts or insulation faults and 7 for other reasons.

4.3. *Field quality performance*

4.3.1. *Strategy*

As in the RHIC production, all magnets were measured at room temperature, and a sample has been measured at 1.9 K. Magnetic measurements at room temperature were carried out at two stages of the assembly, i.e. after the collaring (collared coil) and after the welding of the shrinking cylinder (cold mass). At the beginning of the production, all magnets were measured at 1.9 K with a static load-line and with a standard machine cycle. Once solid warm–cold correlations had been established, a sampling of 7–15% was carried out over the five year production. A total of 200 magnets, corresponding

to 16% of the production, have been measured at 1.9 K.

4.3.2. *Systematic values*

The main novelties of the field quality control in the LHC dipoles with respect to previous machines are the even normal multipoles (quadrupole, octupole) which become allowed multipoles in the twin collar geometry. The iron yoke has been carefully shaped to minimize the impact of saturation [53] using numerical simulations; this optimization procedure has defined the position and the size of the holes in the iron, similarly to what was done in RHIC. The final prototypes showed a systematic quadrupole and octupole outside the targets, and a fine-tuning of both multipoles was carried out by reshaping the ferromagnetic insert between the collars and the yoke (see Fig. 15), using both simulations and a dedicated experiment [54]. The final insert chosen for the production has been shown to give systematic values within targets and no further corrective actions have been necessary during the production (see Figs. 23 and 24).

Concerns about the presence of a nonzero systematic b_4 inducing strong detuning triggered the insertion of octupolar correctors in half of the dipole cold masses; nevertheless, the production has shown very stable values close to zero (see Fig. 24).

The steering of the odd normal components (b_3 sextupole, b_5 decapole, b_7 14th pole; see Figs. 26 and 27) has also required corrective actions [55], as for the RHIC production [56]. Here the situation is more complicated since any change affects at the same time three multipoles and the main field, i.e. one has to control four variables at the same time.

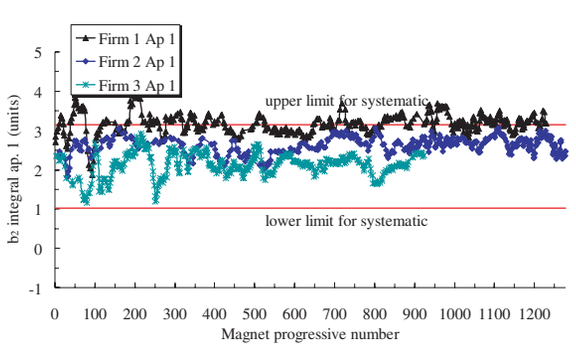

Fig. 23. Evolution of b2 measured in aperture 1 during the production of 1276 dipoles, separated by the assembler (warm magnetic measurements in the cold mass, running average of five magnets per firm). The target limits for the global average are shown in red.

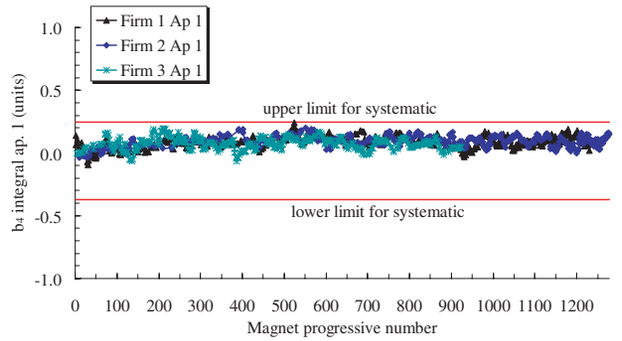

Fig. 24. Evolution of b4 measured in aperture 1 during the production of 1276 dipoles, separated by the assembler (warm magnetic measurements in the cold mass, running average of five magnets per firm). The target limits for the global average are shown in red.

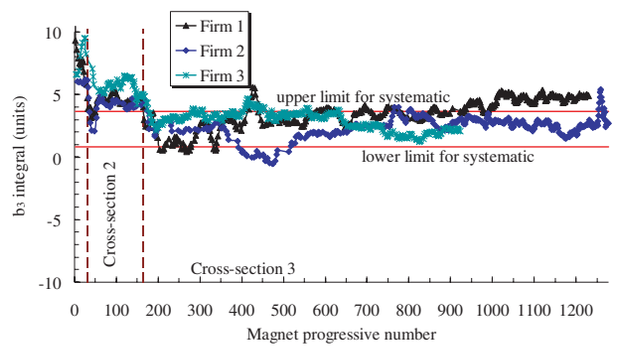

Fig. 25. Evolution of b3 measured in aperture 1 during the production of 1276 dipoles, separated by the assembler (warm magnetic measurements in the cold mass, running average of five magnets per firm). The target limits for the global average are shown in red.

At the beginning of the production both b_3 and $b_5$were outside the target values by a sizeable value (see Figs. 25 and 26), giving an unacceptably large chromaticity at collision energy, beyond the capability of the sextupole correctors. The origin of this discrepancy was due both to neglected effects in the modeling and to a change in the beam dynamic targets. In the LHC dipole, the effect of deformations on field quality is dominated by the deformation of the thick coil inside the very rigid collars, rather than by the deformation of the collar. This effect accounts for three units of b_3 and one of b_5 [57]. Two corrections were carried out during the production, the first one after the measurement of nine dipoles (implemented in dipole 33) by modifying the shape of the inner layer copper wedges but keeping the same coil size

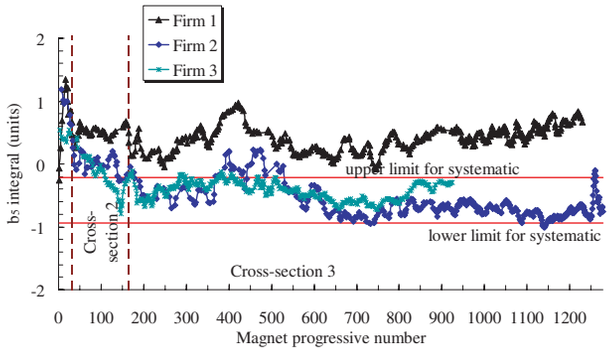

Fig. 26. Evolution of b5 measured in aperture 1 during the production of 1276 dipoles, separated by the assembler (warm magnetic measurements in the cold mass, running average of five magnets per firm). The target limits for the global average are shown in red.

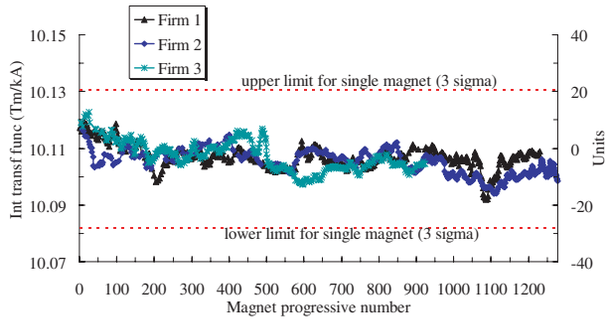

Fig. 27. Evolution of the integrated transfer function during the production, divided by the assembler.

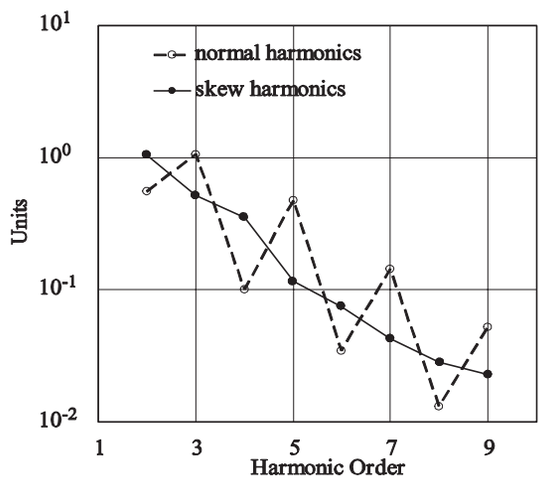

Fig. 28. Random components for LHC dipoles.

to avoid changes in the tooling [55]; the second one after the completion of one octant (154 dipoles) consisted in adding a mid-plane shim, as done for the RHIC dipoles, to further lower $b_3$and b_5 [55].

The agreement between the expected value of the corrections and their actual value is in general within 20%. Both corrections had an unexpected effect on b_7, which was driven out of the target range by 0.2 units, but it was considered acceptable. The final agreement between model and measurements is three units in b_3, one unit in b_5 and 0.5 units in b_7.

4.3.3. *Random components at room temperature*

The variability of the field quality from dipole to dipole, i.e. the so-called random component, is due to the component and assembly tolerances. This variability sets the ultimate limit on the precision available for steering the average values toward the design values over the whole production run. Moreover, random components of multipoles excite resonances which can limit the stability of the beam.

One of the critical field quality parameters is the reproducibility of the integrated transfer function. For the LHC dipoles this quantity has been remarkably stable along all the production (see Fig. 27), and, contrary to the HERA case [58], has shown negligible differences between the cold mass assemblers. The final spread over the entire production at room temperature is ~ 6 units. The option of reducing the transfer function spread via a control of the magnetic length (i.e. changing the longitudinal length of the ferromagnetic laminations) has been used only for a few magnets during the production, just to test the validity of the method.

The random component of b_3 at room temperature is about 1 unit for the ~ 1100 magnets with the same cross section. The spread over all magnets is 1.5 units, compared to a target of 1.4 units. A global view of the random errors at room temperature is given in the semilogarithmic plot shown in Fig. 28. The random components correspond on average to a random positioning of the coil blocks of 0.025 mm rms. This is the lower bound of what is usually considered in simulations [59] for estimating the random errors based on a random movement of the blocks (0.050–0.025 mm). The normal and skew components of the same order have different random components; this "saw-tooth" feature, which was already observed in Tevatron dipoles [60], is somewhat anomalous for the LHC since the skew harmonics show a rather flat

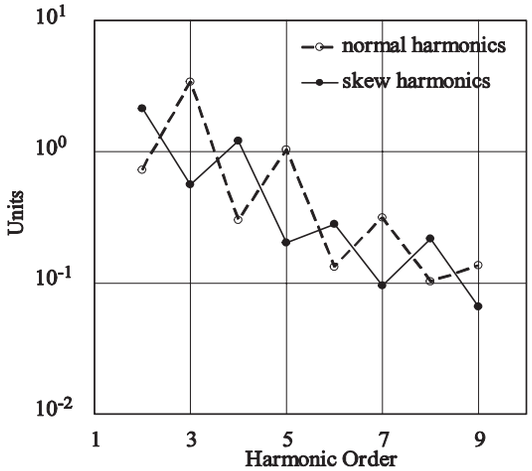

Fig. 29. Random components for HERA dipoles.

Table 6. Amplitude of the random block movements (mm) giving the measured random components.

	Tevatron	HERA	RHIC	LHC	LHC Firm 1
b odd	0.128	0.122	0.052	0.054	0.038
b even	0.052	0.020	0.006	0.012	0.010
a odd	0.070	0.024	0.008	0.018	0.012
a even	0.052	0.058	0.032	0.026	0.022
All	0.065	0.041	0.016	0.025	0.018

behavior in the semilog plot (see the HERA results for comparison in Fig. 29). The amplitude of the random movements corresponding to each family of multipoles [61] for the four machines is given in Table 6. The exceptional results obtained by RHIC in the assembly precision are probably due to the thinner, one-layer coil, and to the simpler design.

The field quality of the LHC dipoles showed a very weak dependence on the cold mass assembler. It has already been pointed out that no signature of the assembler was visible on the transfer function. Some differences have been observed only in two allowed multipoles, b_5 and b_7, and in the skew component a_3. For this reason, the spread inside magnets assembled by the same firm is similar to the global spread for even multipoles, and is $\sim 30\%$ lower for the odd ones (see Table 6). A few trends [62] were observed in the production; some trends in b_3 and a_4 have been traced back to the position of the upper block in the inner coil, close to the pole, as also shown in Fig. 22.

4.3.4. *Warm-cold correlations*

Warm–cold correlations were established during the early part of the production. In all cases the spread of the offset between "warm" and "cold" measurements was smaller than the spread measured at room temperature (see Table 7). In other words, the random part of the field quality is mainly determined by the room temperature measurements. For instance, the spread on b_3 at room temperature is 1–1.5 units and the spread of the warm–cold offset at high field (given by the coil geometry and the iron saturation) is ~ 0.2 units (see Table 7). The offset from room temperature to injection measurement, which is mainly due to the persistent current, is ~ 7 units, and its spread is ~ 0.5 units (see Figs. 30 and 31); this reflects the very good control of cable magnetization. The measured field hysteresis in the magnet is well explained by a model that relies on the magnetization measurements (see Fig. 32 for the b_3 case [63]).

The warm–cold offsets were monitored during the production, where a continuous sampling was taken; they have been remarkably stable (see Fig. 31). This has permitted steering the field quality using room temperature measurements. A negligible impact of the cold mass assembler on the warm–cold offsets was found in most cases, as expected.

Table 7. Spread of the multipoles (1 σ) ar room temperature (RT), and of the offsets between the multipoles measured at 1.9 K at injection energy (inj.) of collision energy (coll.) and room temperature.

	b_2	a_2	b_3	a_3	b_4	a_4	b_5
R.T.	0.59	0.89	1.51	0.39	0.08	0.28	0.54
Inj–R.T.	0.32	0.39	0.40	0.09	0.04	0.09	0.10
Coll.–R.T.	0.33	0.18	0.20	0.10	0.04	0.04	0.07

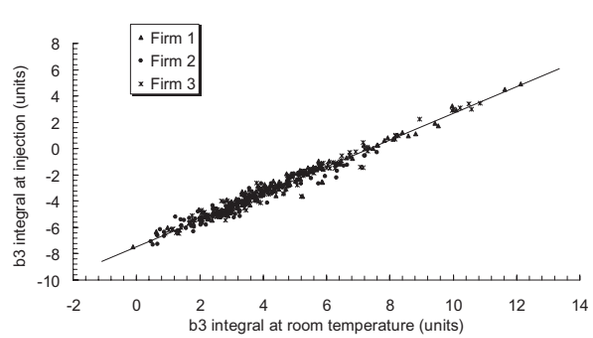

Fig. 30. Warm–cold correlation for b_3 between injection energy and room temperature measurements.

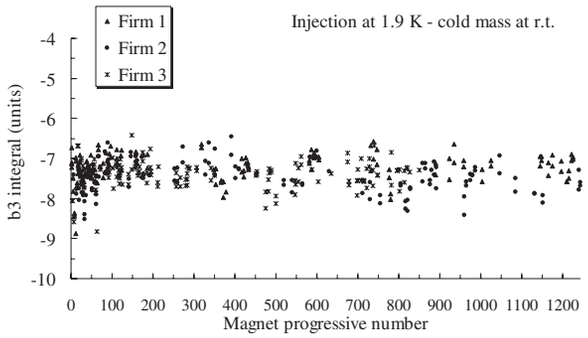

Fig. 31. Evolution of the difference between b_3 measured at injection energy at 1.9 K and at room temperature during the production, divided by the assembler.

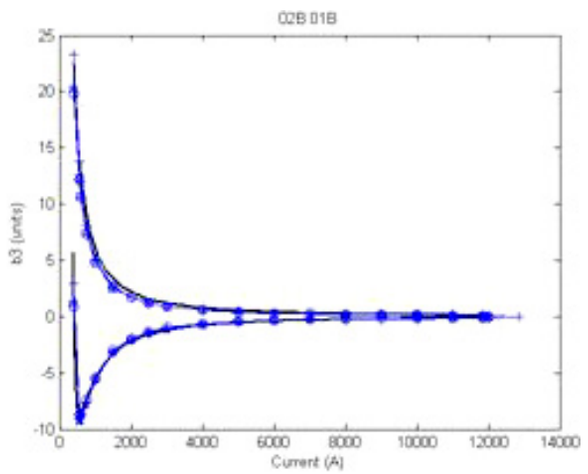

Fig. 32. Measured hysteresis in an LHC dipole (markers) and model based on the magnetization measurements (solid line) [65].

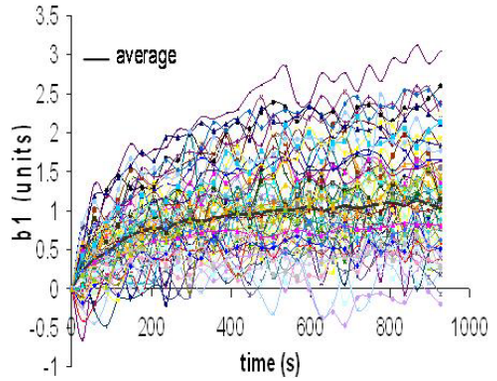

Fig. 33. Measured decay of the main field during the injection plateau measured in 35 LHC dipoles manufactured with cable of producer B [63].

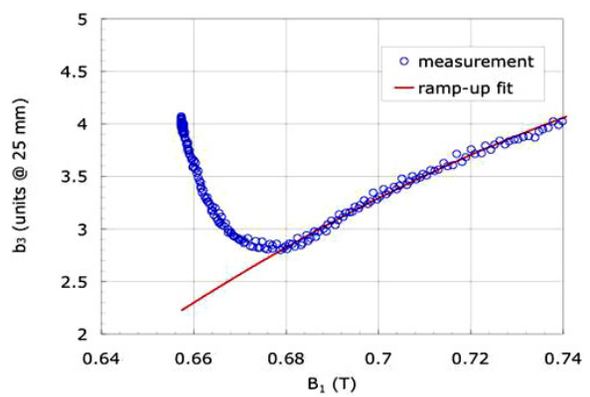

Fig. 34. Evolution of b3 versus main field during the beginning of the ramp (snapback) measured in one LHC dipole [63].

4.3.5. *Dynamic effects*

The foreseen duration of the injection plateau for the LHC at nominal operation is around 20 min. During this time the persistent currents decay about $+1.5$ units (transfer function), $+2$ units (b_3) and -0.35 units (b_5) (see Fig. 33). These values have been measured for ~ 200 dipoles at 1.9 K. When the ramp is started, the decay suddenly disappears and the field harmonics snap back to their original value in a few seconds (see Fig. 34). For the LHC, special probes have been developed to measure these fast phenomena [64], and have been used also for measuring the Tevatron magnets during RUN II [65].

The Tevatron experience showed that the magnetic behavior of superconducting elements gives rise to time-dependent phenomena and loss of reproducibility, which can severely affect machine operation [15]. For the LHC dipoles, a few of them underwent special tests to work out the dependence of the decay on the previous cycle parameters. Results are in qualitative agreement with the experience acquired on previous machines, i.e. that the amplitude of the decay is roughly proportional to the flat top field of the precycle, is smaller for a longer duration of the flat top in the precycle, and gets larger for a shorter preinjection porch.

Different empirical fits have been used for the decay (logarithm, single or double exponential) in the four machines. A similar situation holds for the snapback dependence on the current. A significant result linking the snapback amplitude and its decay constant in the case of an exponential fit was found during the first years of the LHC dipole production;

this scaling law has been proven both for the LHC and Tevatron dipoles [65]. A major effort was carried out to build an LHC field model [66, 67] using all the relevant information and permitting the programming of the circuit magnets before day 1 of commissioning.

4.4. *Quench performance*

The quench performance has been measured on 12 test benches at CERN for all dipoles at 1.9 K [68]. The LHC magnets show little or no training to reach the nominal field, and therefore the standard test used for the early part of the production consisted of two quenches to get to 8.4 T; if this condition was not satisfied, the ultimate value of 9 T had to be reached within nine quenches. Otherwise, the magnet was tested again after a thermal cycle (warm-up and cool-down). These criteria have been updated for the mature phase of the production, replacing the two-quench–8.4 T with a three-quench–8.6 T requirement. They have been established according to: (i) optimizing the time necessary for testing, (ii) minimizing the expected quenches in the tunnel during commissioning, and (iii) detecting magnets with insufficient performance. Fourteen magnets (1.2% of the production) have been returned to the assemblers for insufficient quench performance, and repaired. In the initial phase of the production, one dipole sustained severe damage during the test which provoked the destruction of the coil.

80% of the dipoles reached 8.3 T without or with one quench, and 17% with two quenches. 11% of the dipoles were tested after a thermal cycle: 76% reached 8.3 T without quenches, 19% with one quench, and 4% with two quenches. The histogram of the value of the first and the second quench, and of the first quench after the thermal cycle, is shown in Fig. 35.

The dipoles tested after the thermal cycle had some detraining, i.e. the value of the first quench after the thermal cycle was lower then the value of the last quench before warm-up. 20% of the dipoles had no detraining, 33% had a lower field of 0–0.3 T, 33% of 0.3–0.6 T, 12% of 0.6–1.0 T, and 2% of up to 1.4 T. These results must be read taking into account that only the "bad" dipoles were tested after a thermal cycle, and therefore the statistics could be biased.

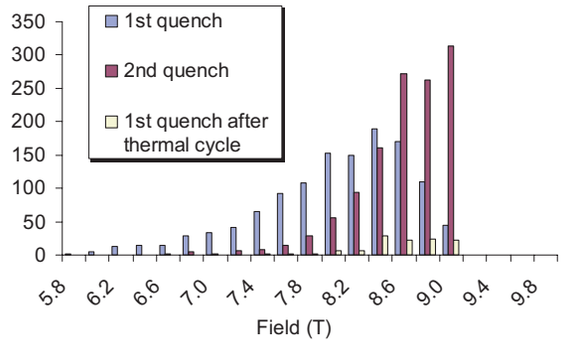

Fig. 35. First and second quench levels (all LHC dipoles), and first quench after the thermal cycle (a sample of 130 dipoles).

Quench longitudinal localization through a quench antenna has been carried out for $\sim 1/6$ of the dipoles. Results show that 85–90% of the quenches originated in the coil ends. This proves that the level of prestress on the straight part of the coil was not the main limitation on the quench performance.

4.5. *Installation strategy*

Contrary to the original baseline, installation was started when a large stock of measured magnets was available. Moreover, the magnetic measurements at room temperature provided the main field quality features of the dipoles, some months in advance of their arrival at CERN. For these reasons the Magnet Evaluation Board [69], in charge of the allocation of the magnets in the ring, has faced the "dream" situation of being able to sort practically all the dipoles in the ring to maximize the machine performance. To be more precise, the dipoles were produced in four families (i.e. according to the corrector package and the diode polarity) and therefore the sorting had to be done within these families, and not all over the machine.

The first two types of cross sections were installed in the first octant to minimize the spread on b_3. Both a local compensation and a compensation at a π or 2π betatron phase advance have been used. This possibility have also been used in the other sectors to further reduce the spread of b_3 and a_2 with respect to the original targets, with a gain of the order of a factor 2–3 on the required orbit corrector strength, coupling resonance and vertical dispersion, and third order resonance driving terms.

A more significant improvement in the machine performance has been obtained by sorting the dipoles

according to the measured shape to maximize the mechanical aperture. Dipoles with shapes above tolerances have been allocated to slots where the beam envelope given by the optical functions is smaller, as the mid-cell positions. This action eliminated any aperture limitations on the main dipoles. No sorting has been done on the measured quench performance.

5. Outlook for Future Accelerator Magnets

The 9.7 T short sample field of the LHC dipoles is close to the ultimate limit of what can be done with Nb–Ti, which has been the "workhorse" superconducting material for accelerator magnets in the past 25 years. The record for a Nb–Ti dipole belongs to the 88 mm aperture dipole used in the cable test station at CERN [70], which has a two-layer $\cos\theta$ design with a 16.7 mm cable width, and a short sample field of 10.15 T. It reached 10.09 T after a short training period and is routinely used to measure the cable critical current at 10 T. Similar performances were obtained by the D19 model in LBL, having a maximum quench field of 10.06 T with a strongly graded two-layer coil of $2 * 12$ mm thickness [71].

A 10% increase to get an 11 T short sample limit would require doubling the coil width with respect to the LHC dipoles (see Fig. 36). Since ~ 14 T is the critical field at 0 K and at zero current density for the Nb–Ti, the only possibility of achieving higher fields is to use materials with higher performance in terms of critical field and current density (see Fig. 37).

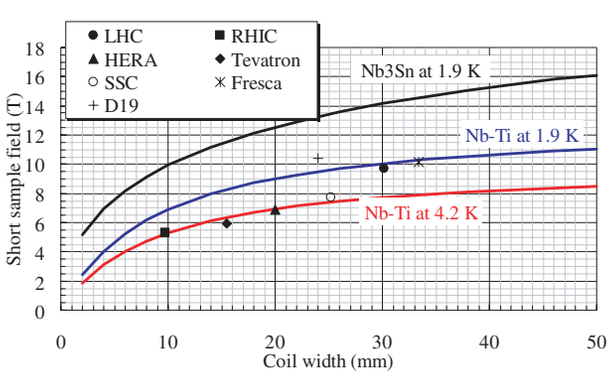

Fig. 36. Short sample field versus coil width for five dipoles (markers), and estimate for an ironless $\cos\theta$ coil at 4.2 K (red line) and at 1.9 K (blue line), with a filling factor of 0.3. The same Nb-Ti cable properties have been assumed for all dipoles. The $\cos\theta$ estimate is also given for the best Nb3Sn conductor available today.

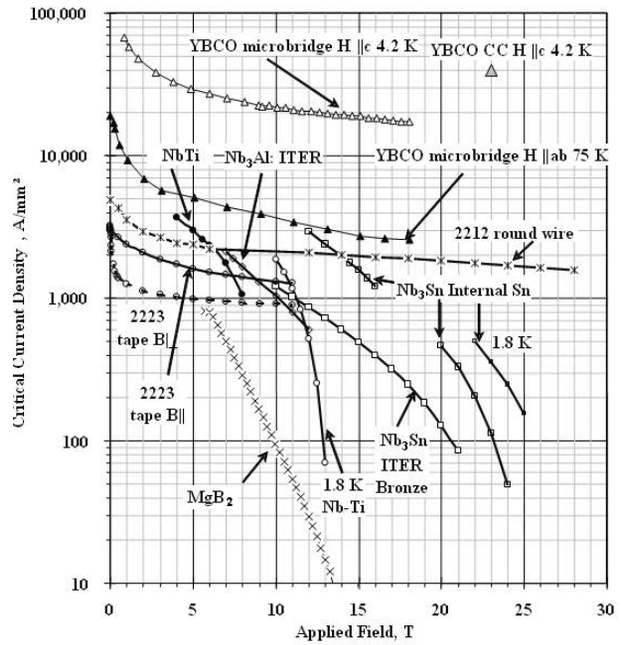

Fig. 37. Critical current of several types of superconductors versus magnetic field [78].

At the beginning of the 1990s, when the Nb_3Sn prototype for the LHC [25] was built, the critical current density at 10 T was only marginally larger than in Nb–Ti. Now, after 20 years of R&D in superconducting materials, a conductor bearing up to 3000 A/mm^2 at 12 T and 4.2 K is available, with a filament size of the order of 50 μm [72]. Using this cable, the fields reachable in a $\cos\theta$ dipole are shown in Fig. 36: a coil width of 30–45 mm can provide short sample fields in the range of 14–16 T.

The main issues for Nb_3Sn are its brittleness, the degradation induced by strain, and instabilities related to flux jumps [73]. They can be resolved by optimizing the design and the treatment of the strand, and by a clever mechanical structure. Besides the collars, invented for the Tevatron dipoles and used in all accelerator dipoles except RHIC, an alternative structure based on an aluminum shell pretensioned with bladders and keys has been proposed. This structure allows the highest peak stress to be reached at the end of cool-down and not during collaring. It has been successfully implemented in Nb_3Sn dipoles and quadrupoles [74, 75]. Another innovation in the coil layout is a design where non-keystoned Rutherford cables are arranged in rectangular blocks [76, 77].

Up to now, Nb_3Sn has been routinely used in solenoids to reach fields in the range of 10–20 T [79], but Nb_3Sn magnets have never been used in accelerators. Nevertheless, short models with accelerator-like field quality were built during the 1990s, attaining fields in the range of 11–13 T [80, 81]. This R&D has rapidly evolved in the last few years. Simple designs such as racetrack dipole coils, without field quality, have been able to reach a bore field of 16 T [75] in a 1 m model. Recent results have also shown that 4-m-long Nb_3Sn quadrupole coils with a peak field of 12 T can be successfully manufactured [82]. FNAL [83] and the Lawrence Berkeley Laboratory [77] are today aiming at building Nb_3Sn dipoles with $\sim$40 mm apertures with a coil width of 30–45 mm, and a short sample field in the range of 12–15 T. Nb_3Sn quadrupoles with a peak field in the range of 12–15 T could be used for the upgrade of the quadrupoles in the LHC interaction regions, and this would provide the first test of the reliability of Nb_3Sn magnets in an accelerator.

The discovery that high temperature superconductors such as YBCO and Bi2212 have critical fields well beyond 50 T when operated at LHe temperature opens up new possibilities for accelerator uses. The difficulties in fabricating coils with the material are very similar to Nb_3Sn, and going to fields in the range of 20–50 T poses really challenging problems for the magnet designer. But the fact that these materials can have high radiation resistance, can work at high temperature or can achieve very high fields may offer new applications such as low beta quads for interaction regions in accelerators or for providing intense cold muon beams for neutrino factories or muon colliders. Ever since Zeeman's early work, higher magnet fields have led the way to new physics, so the promise is still high!

Acknowledgments

A. T would like to acknowledge the excitement and fun of working with Bob Wilson and the contributions of the many extremely talented people who worked on the Tevatron. We would both like to thank all the colleagues who were involved in the LHC dipole models, prototypes and production.

References

[1] R. R. Wilson, E. L. Goldwasser, D. A. Edwards, W. B. Fowler, B. P. Strauss, G. Biallas, W. B. Hanson, D. F. Sutter, P. J. Reardon and P. C. Vander Arend, The Energy Doubler Design Study: a progress report, *Fermilab Phys. Notes* **FN-263**, 4 (1974).

[2] T. Elioff, W. Gilbert, G. Lamberston and R. Meuser, *IEEE Trans. Magn.* **11**, 447 (1975).

[3] J. R. Sanford, Isabelle, a proton–proton colliding beam facility, *BNL Report* **50718** (1978).

[4] M. N. Wilson, *Superconducting Magnets* (Clarendon, Oxford, 1983).

[5] H. E. Edwards, *Ann. Rev. Nucl. Part. Sci.* **35**, 605 (1985).

[6] R. Palmer and A. V. Tollestrup, *Ann. Rev. Nucl. Part. Sci.* **34**, 247 (1984).

[7] B. P. Strauss, R. H. Remsbottom, P. J. Reardon, C. W. Curtist and W. K. McDonald, *IEEE Trans. Magn.* **13**, 487 (1977).

[8] D. C. Larbalestier, *IEEE Trans. Nucl. Sci.* **30**, 3299 (1983).

[9] K. Koepke, G. Kalbfleisch, W. Hanson, A. Tollestrup, J. O'Meara and J. Saarivirta, *IEEE Trans. Magnetics***15**, 658 (1979).

[10] R. Hanft, B. C. Brown, W. E. Cooper, D. A. Gross, L. P. Michelotti, E. E. Schmidt and F. Turkot, *IEEE Trans. Nucl. Sci.***30**, 3381 (1983).

[11] M. Wake, D. A. Gross, M. Kumada, D. Blatchley and A. V. Tollestrup, *IEEE Trans. Nucl. Sci.* **26**, 3894 (1983).

[12] E. E. Schmidt, B. C. Brown, W. E. Cooper, H. E. Fisk, D. A. Gross, R. Hanft, S. Ohnuma and F. T. Turkot, *IEEE Trans. Nucl. Sci.* **30**, 3384 (1983).

[13] B. C. Brown, W. E. Cooper, J. D. Garvey, D. A. Gross, R. Hanft, K. P. Kaczar, J. E. Pachnik, C. W. Schmidt, E. E. Schmidt and F. Turkot, *IEEE Trans. Nucl. Sci.* **30**, 3608 (1983).

[14] C. P. Bean, *Rev. Mod. Phys.* **36**, 31 (1964).

[15] G. V. Velev, G. Annala, P. Bauer, R. Carcagno, J. Di Marco, H. Glass, R. Hanft and R. Kephart, in *Particle Accelerator Conference* (2003), p. 1972.

[16] M. Wake, D. Gross, R. Yamada and D. Blatchley, *IEEE Trans. Magne.* **15**, 141 (1979).

[17] B. Peters, L. Harris, J. Saarivirta and A. Tollestrup, *IEEE Trans. Magne.* **15**, 134 (1979).

[18] G. Biallas, J. Finks, B. Strauss, M. Kuchnir, W. Hanson, E. Kneip, H. Hinterberger, D. Dewitt and R. Powere, *IEEE Trans. Magne.* **15**, 131 (1979).

[19] P. C. Vander Arend and W. B. Fowler, *IEEE Trans. Nucl. Sci.* **20**, 119 (1973).

[20] R. Stiening, R. Flora, R. Lauckner and G. Tool, *IEEE Trans. Magne.* **15**, 670 (1979).

[21] G. A. Voss and B. H. Wiik, *Ann. Rev. Nucl. Part. Sci.* **44**, 413 (1994).

[22] E. Apostolescu, R. Bandelmann, H. Boettcher, I. Borchardt, G. Deppe, K. Escherich, H. Kaiser, M. Leenen, O. Peters, H. Poggensee, S. L. Wipf and S. Wolff, *IEEE Trans. Magne.* **28**, 689 (1992).

[23] M. A. Harrison, The RHIC Project, *BNL Rep.* **49794** (1994).

[24] R. Perin, D. Leroy and G. Spigo, *IEEE Trans. Magne.* **25**, 1632 (1989).

[25] H. ten Kate, A. den Ouden, D. ter Avest, S. Wessel, R. Dubbeldam, W. van Emden, C. Daum, M. Bona and R. Perin, *IEEE Trans. Magne.* **27**, 1996 (1991).

[26] M. Bona, R. Perin, E. Acerbi and L. Rossi, *IEEE Trans. Magne.* **32**, 2051 (1996).

[27] J. Billan, M. Bona, L. Bottura, D. Leroy, O. Pagano, R. Perin, D. Perini, F. Savary, A. Siemko, P. Sievers, G. Spigo, J. Vlogaert, L. Walckiers and C. Wyss, *IEEE Trans. Appl. Supercond.* **9**, 1039 (1999).

[28] L. Rossi, *IEEE Trans. Appl. Supercond.* **12**, 219 (2002).

[29] O. Bruning, P. Collier, P. Lebrun, S. Myers, R. Ostojic, J. Poole and P. Proudlock, *CERN Rep.* **2004003** (2004).

[30] R. Palmer and A. Tollestrup, *Fermilab* **TM-1251**, 67 (1984).

[31] D. Tommasini, Insulation in the LHC magnets, *LHC Proj. Rep.*, in preparation.

[32] S. Russenschuck, *CERN Rep.* **99-01**, 82 (1999).

[33] Technical specification for the LHC dipoles, IT-2997/LHC/LHC (2001).

[34] P. Fessia, D. Perini, R. Vuillerment and C. Wyss, *LHC Proj. Note* **288** (2002).

[35] A. Devred, T. Bush, R. Coombes, J. DiMarco, C. Goodzeit, J. Kuzminski, M. Puglisi, P. Radusewicz, P. Sanger, R. Schermer, G. Spigo, J. Thompkins, J. Turner, Z. Wolf, Y. Yu and H. Zheng, *AIP Conf. Proc.* **249**, 1309 (1992).

[36] P. Ferracin, W. Scandale, E. Todesco and D. Tommasini, *IEEE Trans. Appl. Supercond.* **12**, 1705 (2002).

[37] N. Siegel, D. Tommasini and I. Vanenkov, *LHC Proj. Rep.* **173** (1998).

[38] N. Andreev, K. Artoos, E. Casarejos, T. Kurtyka, C. Rathjen, D. Perini, N. Siegel, D. Tommasini, I. Vanenkov, *LHC Proj. Rep.* **179** (1998).

[39] P. Ferracin, W. Scandale, E. Todesco and D. Tommasini, *Phys. Rev. STAB* **5**, 062401 (2002).

[40] M. Bajko, R. Chamizo, C. Charrondiere, A. Kuzmin and F. Savary, *IEEE Trans. Appl. Supercond.* **16**, 429 (2006).

[41] Ph. Lebrun, *IEEE Trans. Appl. Supercond.* **10**, 1500 (2000).

[42] N. Bourcey, O. Capatina, V. Parma, A. Poncet, P. Rohmig, L. Serio, B. Skoczen, J.-P. Tock and L. R. Williams, *AIP Conf. Proc.* **710**, 487 (2004).

[43] F. Seyvet, J.-B. Jeanneret, A. Poncet, D. Tommasini, J. Beauquis, E. D. Fernandez Cano and E. Wildner, in *Particle Accelerator Conference* (2005), p. 2675.

[44] F. Rodríguez-Mateos, K. Dahlerup-Petersen, R. Denz Milani and F. Tegenfeldt, *IEEE Trans. Appl. Supercond.* **14**, 251 (2004).

[45] A. Verweij and A. Ghosh, *IEEE Trans. Appl. Supercond.* **17**, 1454 (2007).

[46] S. Le Naour, L. Oberli, R. Wolf, R. Puzniak, A. Szewczyk, A. Wisniewski, H. Fikis, M. Foitl and H. Kirchmayr, *IEEE Trans. Appl. Supercond.* **9**, 1763 (1999).

[47] B. Bellesia, F. Bertinelli, P. Fessia, G. Gubello, C. Lanza, W. Scandale and E. Todesco, *CERN LHC Proj. Rep.* **630** (2003).

[48] I. Vanenkov and C. Vollinger, in *Particle Accelerator Conference* (2003), p. 1951.

[49] B. Bellesia, F. Bertinelli, C. Santoni and E. Todesco, *IEEE Trans. Appl. Supercond.* **16**, 196 (2006).

[50] R. Gupta, M. Anerella, J. Cozzolino, D. Fisher, A. Ghosh, A. Jain, W. Sampson, J. Schmalzle, P. Thompson, P. Wanderer and E. Willen, *Proc. MT-15 Conference.*

[51] C. Vollinger and E. Todesco, *IEEE Trans. Appl. Supercond.* **16**, 204 (2006).

[52] B. Bellesia, G. Molinari, C. Santoni, W. Scandale and E. Todesco, *IEEE Trans. Appl. Supercond.* **16**, 208 (2006).

[53] C. Vollinger, *CERN Rep.* **99-01**, 93 (1999).

[54] L. Bottura, S. Redaelli, V. Remondino, S. Sanfilippo, F. Savary, W. Scandale and E. Todesco, in *Eighth European Particle Accelerator Conference* (2002), p. 2427.

[55] E. Todesco, B. Bellesia, L. Bottura, A. Devred, V. Remondino, S. Pauletta, S. Sanfilippo, W. Scandale, C. Vollinger and E. Wildner, *IEEE Trans. Appl. Supercond.* **14**, 177 (2004).

[56] R. Gupta, M. Anerella, J. Cozzolino, B. Erickson, A. Greene, A. Jain, S. Kahn, E. Kelly, G. Morgan, P. Thompson, P. Wanderer and E. Willen, *IEEE Trans. Magne.* **32**, 2069 (1996).

[57] P. Ferracin, O. Pagano, V. Remondino, W. Scandale, E.Todesco and D. Tommasini, *IEEE Trans. Appl. Supercond.* **12**, 1727 (2002).

[58] R. Meinke, *IEEE Trans. Magn.* **27**, 1728 (1990).

[59] R. Gupta, *Part. Accel.* **54**, 379 (1996).

[60] J. Herrera, R. Hogue, A. Prodell, P. Wanderer and E. Willen, in *Particle Accelerator Conference* (1985), p. 3689.

[61] B. Bellesia, E. Todesco, in *European Particle Accelerator Conference* (2006), p. 2601.

[62] E. Todesco, B. Bellesia, P. Hagen, C. Vollinger, *IEEE Trans. Appl. Supercond.* **16**, 419 (2006).

[63] T. Pieloni, S. Sanfilippo, L. Bottura, M. Haverkamp, A. Tikhov, E. Effinger, E. Benedico and N. Smirnov, *IEEE Trans. Appl. Supercond.* **14**, 1822 (2004).

[64] G. Ambrosio, P. Bauer, L. Bottura, M. Haverkamp, T. Pieloni, S. Sanfilippo and G. Velev, *IEEE Trans. Appl. Supercond.* **15**, 1217 (2005).

[65] S. Sanfilippo, talks given at field quality working group, http://www.cern.ch/fqwg

[66] N. Sammut, L. Bottura and J. Micallef, *Phys. Rev. STAB* **9**, 012402 (2006).

[67] N. Sammut, L. Bottura, P. Bauer, G. Velev, T. Pieloni and J. Micallef, *Phys. Rev. STAB* **10**, 082802 (2007).

[68] A. Siemko and P. Pugnat, *IEEE Trans. Appl. Supercond.* **17**, 1091 (2007).
[69] P. Bestmann, L. Bottura, N. Catalan-Lasheras, S. Fartoukh, S. Gilardoni, M. Giovannozzi, J.-B. Jeanneret, M. Karppinen, A. Lombardi, K.-H. Meß, D. Missiaen, M. Modena, R. Ostojic, Y. Papaphilippou, P. Pugnat, S. Ramberger, S. Sanfilippo, W. Scandale, F. Schmidt, N. Siegel and A. Siemko, in *Particle Accelerator Conference* (2007), p. 3739.
[70] D. Leroy, G. Spigo, A. Verweij, H. Boschman, R. Dubbeldam and J. Pelayo, *IEEE Trans. Appl. Supercond.* **10**, 178 (2000).
[71] D. Dell'Orco, S. Caspi, J. O'Neill, A. Lietzke, R. Scanlan, C. B. Taylor and A. Wandersforde, *IEEE Trans. Appl. Supercond.* **3**, 637 (1993).
[72] D. Dietderich, E. Barzi, A. Ghosh, N. Liggins and H. Higley, *IEEE Trans. Appl. Supercond.* **17**, 1481 (2007).
[73] A. Zlobin, V. Kashikhin and E. Barzi, *IEEE Trans. Appl. Supercond.* **16**, 1308 (2006).
[74] S. Caspi, D. Dietderich, P. Ferracin, S. Gourlay, A. Hafalia, R. Hannaford, A. Lietzke, A. McInturff, G. Sabbi, A. Ghosh, A. Andreev, E. Barzi, R. Bossert, V.; Kashikhin, I. Novitski, G. Whitson and A. Zlobin, *IEEE Trans. Appl. Supercond.* **17**, 1122 (2007).
[75] A. Lietzke, A. Bartlett, P. Bish, S. Caspi, L. Chiesa, D. Dietderich, P. Ferracin, S. Gourlay, M. Goli, R. Hafalia, H. Higley, R. Hannaford, W. Lau, N. Liggens, S. Mattafirri, A. McInturff, M. Nyman, G. Sabbi, R. Scanlan and J. Swanson, *IEEE Trans. Appl. Supercond.* **14**, 345 (2004).
[76] G. Ambrosio, N. Andreev, E. Barzi, P. Bauer, D. Chichili, K. Ewald, L. Imbasciati, V. Kashikhin, S. Kim, P. Limon, I. Novitski, J. P. Ozelis, R. Scanlan, G. Sabbi and A. Zlobin, *IEEE Trans. Appl. Supercond.* **11**, 2172 (2001).
[77] P. Ferracin, S. Bartlett, S. Caspi, D. Dietderich, S. Gourlay, A. Hafalia, C. Hannaford, A. Lietzke, S. Mattafirri, A. Mcinturff, G. Sabbi, *IEEE Trans. Appl. Supercond.* **16**, 378 (2006).
[78] P. Lee, http://magnet.fsu.edu/∼lee/plot/plot.htm
[79] T. Kiyoshi, S. Matsumoto, M. Kosuge, M. Yuyama, H. Nagai, F. Matsumoto and H. Wada, *IEEE Trans. Magn.* **12**, 470 (2002).
[80] H. J. ten Kate *et al.*, *IEEE Trans. Magn.* **27**, 1996 (1991).
[81] R. Benjegerdes *et al.*, *Particle Accelerator Conference* (1999), p. 3233.
[82] P. Ferracin, G. Ambrosio, M. Anerella, E. Barzi, S. Caspi, D. Cheng, D. Dietderich, S. Gourlay, A. Hafalia, C. Hannaford, A. Lietzke, A. Nobrega, G. Sabbi, J. Schmalzle, P. Wanderer and A. Zlobin, *IEEE Trans. Appl. Supercond.* **17**, 1023 (2007).
[83] F. Nobrega, A. V. Zlobin, G. Ambrosio, N. Andreev, E. Barzi, R. Bossert, R. Carcagno, S. Feher, V. S. Kashikhin, V. V. Kashikhin, M. J. Lamm, I. Novitski, Yu. Pischalnikov, C. Sylvester, M. Tartaglia, D. Turrioni and R. Yamada, *IEEE Trans. Appl. Supercond.* **17**, 1031 (2007).

Alvin Tollestrup came to Fermilab during the initial design of the Tevatron and helped develop the first superconducting accelerator magnets. He was co-spokesman of the CDF detector during its construction and initial operation and participated in the discovery of the top quark. Lately he helped with the design study for a muon collider. He is grateful for having a career that witnessed the discovery of the pi meson and helped with the discovery of the top!

Ezio Todesco has been working on beam dynamics in particle accelerators for 10 years, mainly on issues related to resonances, perturbative tools, chaotic motion and long-term stability. Since 1998 he has been working at CERN in the design and construction of the superconducting magnets for the Large Hadron Collider (LHC).